Supplementary Information For

Therapeutic ultrasound enables rapid and robust activation of ROS-responsive prodrugs in vivo

Shuyu Huan[#,1,2], Zixi Li[#,2,3], Tianzhen Sun[#,4], Bingru Li[1], Xunbin Wei[2,3,4,5], Xiaoda Yang[1], Guoquan Liu[2,3*]

Table of content

1. Chemical Synthetic Methods

1.1 General synthetic route of DHBC-motif compounds 1−2

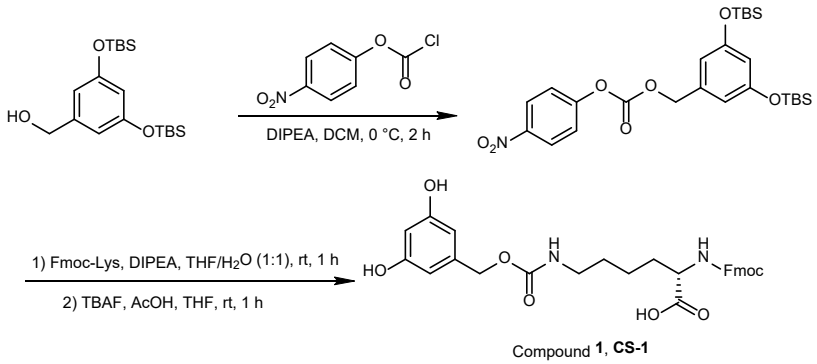

Scheme S1. Synthetic route of compound 1.

Synthesis of compound **1**: 3,5-Bis(tert-butyldimethylsilyloxy)benzyl alcohol (5.5 g, 15 mmol) was dissolved in dichloromethane (DCM, 100 mL) under an ice–water bath. N,N-Diisopropylethylamine (DIEA, 5.8 g, 45 mmol) was added, followed by the slow addition of 4-nitrophenyl chloroformate (12.5 g, 37.5 mmol). The mixture was stirred at room temperature stirred for 2 h. Upon completion, the reaction was quenched with ice water, and the mixture was extracted with DCM (3 × 20 mL), dried over anhydrous $MgSO_4$, filtered, and concentrated under reduced pressure. The crude product was purified by flash chromatography (cyclohexane/ethyl acetate = 90:10, v/v) to give the desired intermediate, 3,5-bis(tert-butyldimethylsilyloxy)benzyl (4-nitrophenyl) carbonate (16.9 g, 85% yield, white solid).

Fmoc-Lysine (0.37 g, 1 mmol) and DIEA (340 μL, 2 mmol) were dissolved in THF/H_2O (30 mL, v/v = 1:1). The above intermediate (0.53 g, 1 mmol) was added, and the mixture was stirred at room temperature for 1 h. Then the mixture was extracted with ethyl acetate, and the organic phase was washed and dried over anhydrous $MgSO_4$, filtered, and concentrated under reduced pressure. The crude product was redissolved in tetrabutylammonium fluoride (TBAF, 1 M in THF, 3 mL, 3 mmol). The mixture was adjusted to slightly acidic pH with acetic acid (AcOH), stirred for 1 h, and evaporated to dryness under reduced pressure. The crude product was purified by flash chromatography (DCM/MeOH = 25:1, followed by DCM/MeOH = 10:1, v/v) to afford compound **1** (0.32 g, 60% yield, white solid). HRMS (ESI^-) m/z: calculated for $C_{29}H_{31}N_2O_8$ ($[M-H]^-$): 533.1929; found: 533.1919.

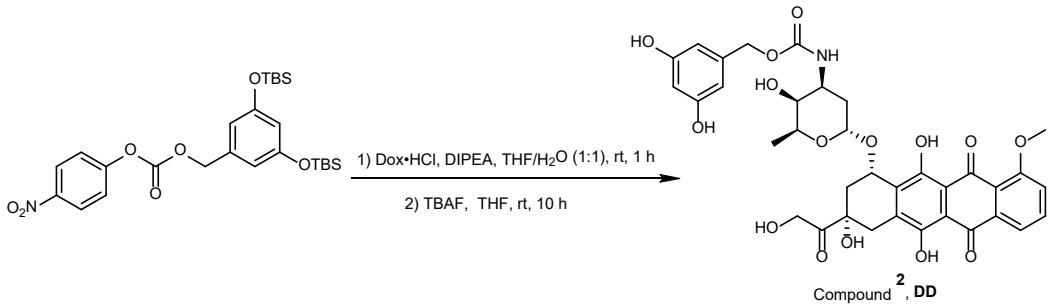

Scheme S2. Synthetic route of compound 2.

Doxorubicin hydrochloride (0.41 g, 1 mmol) and DIEA (340 μL, 2 mmol) were dissolved in THF/H_2O (30 mL, v/v = 1:1). 3,5-Bis(tert-butyldimethylsilyloxy)benzyl (4-nitrophenyl) carbonate (0.53 g, 1 mmol) was added, and the mixture was stirred at room temperature for 1 h. Upon completion, the mixture was extracted with ethyl acetate, and the organic layer was washed and dried over anhydrous $MgSO_4$, filtered, and concentrated under reduced pressure. The crude product was redissolved in TBAF (1 M in THF, 3 mL, 3 mmol), and the mixture was adjusted to slightly acidic pH with acetic acid (AcOH)

and stirred for 10 h, stirred for 1 h, and evaporated to dryness under reduced pressure. The crude product was purified by flash chromatography (DCM/MeOH = 9:1, v/v) to afford compound **2** (0.32 g, 60% yield, red solid). ^{1}H NMR (400 MHz, $CDCl_3$) δ 13.92 (s, 1H), 13.13 (s, 1H), 7.98 (d, *J* = 7.6 Hz, 1H), 7.76 (t, *J* = 8.0 Hz, 1H), 7.37 (d, *J* = 8.4 Hz, 1H), 6.39 (d, *J* = 2.3 Hz, 2H), 6.23 (d, *J* = 2.3 Hz, 1H), 5.51 (d, *J* = 3.7 Hz, 1H), 5.25 (d, *J* = 9.0 Hz, 2H), 4.96 – 4.84 (m, 2H), 4.77 (s, 2H), 4.57 (s, 1H), 4.22 – 3.35 (m, 7H), 3.17 (s, 1H), 2.90 (s, 2H), 2.34 (d, *J* = 14.7 Hz, 2H), 2.17 (dd, *J* = 14.6, 3.8 Hz, 1H), 1.84 (ddt, *J* = 26.1, 13.2, 7.3 Hz, 2H), 1.34 – 1.24 (m, 4H), 0.94 (s, 18H), 0.16 (s, 12H). ^{13}C NMR (101 MHz, $CDCl_3$) δ 213.91, 186.84, 186.46, 160.96, 156.55, 156.15, 155.53, 155.49, 138.23, 135.73, 135.33, 133.57, 120.67, 119.78, 118.46, 112.86, 111.58, 111.44, 111.29, 100.73, 76.57, 69.62, 69.55, 67.33, 66.45, 65.54, 56.60, 47.05, 35.58, 33.89, 30.17, 25.68, 25.64, 18.15, 16.85.

1.2 General synthetic route of DMOBC-motif compound 3

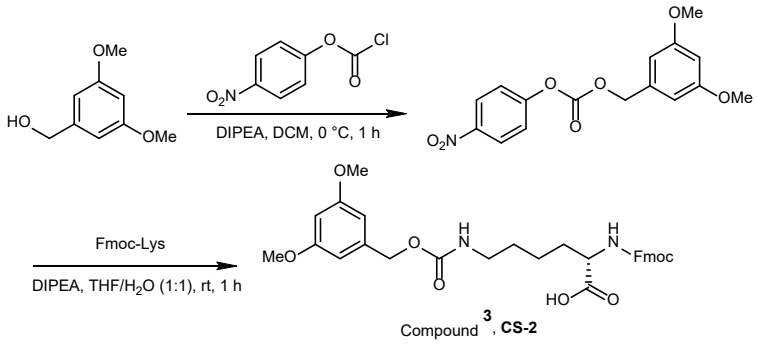

Scheme S3. Synthetic route of compound 3.

3,5-Dimethoxybenzyl alcohol (2.5 g, 15 mmol) was dissolved in DCM (100 mL) under an ice–water bath. DIEA (5.8 g, 45 mmol) was added, followed by the slow addition of 4-nitrophenyl chloroformate (12.5 g, 37.5 mmol). The mixture stirred at room temperature for 2 h. Upon completion, the reaction was quenched with ice water, and the mixture was extracted with DCM (3 × 20 mL), dried over anhydrous $MgSO_4$, filtered, and concentrated under reduced pressure. The crude product was purified by flash chromatography (cyclohexane/ethyl acetate = 90:10, v/v) to give the desired intermediate, 3,5-dimethoxybenzyl (4-nitrophenyl) carbonate (4.5 g, 90% yield).

Fmoc-Lysine (0.37 g, 1 mmol) and DIEA (340 μL, 2 mmol) were dissolved in THF/H_2O (30 mL, v/v = 1:1). The above intermediate (0.33 g, 1 mmol) was added, and the mixture was stirred at room temperature for 1 h. Then the mixture was extracted with ethyl acetate, washed, dried over anhydrous $MgSO_4$, filtered, and concentrated under reduced pressure. The crude product was purified by flash chromatography (DCM/MeOH = 25:1, followed by DCM/MeOH = 10:1, v/v) to afford compound **3** (0.45 g, 80% yield, white solid). HRMS (ESI^-) m/z: calculated for $C_{31}H_{33}N_2O_8$ ($[M-H]^-$): 561.2242; found: 561.2231.

1.3 General synthetic route of azide-motif compound 6

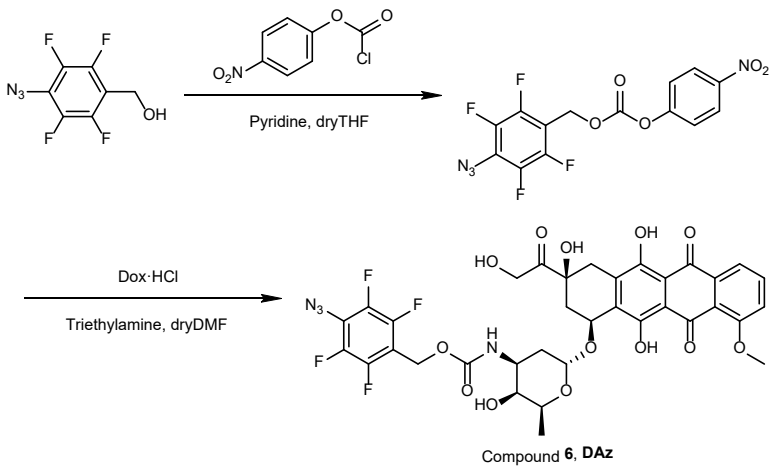

Scheme S4. Synthetic route of compound 6.

Compound **6** was synthesized following previously reported procedures and the characterization matched with the previously reported data[1]. ^{1}H NMR (400 MHz, $CDCl_3$) δ 13.58 (s, 1H), 12.79 (s, 1H), 7.57 (d, *J* = 7.6 Hz, 1H), 7.46 (q, *J* = 8.0 Hz, 1H), 7.11 (d, *J* = 8.5 Hz, 1H), 6.89 (s, 1H), 5.80 (d, *J* = 8.4 Hz, 1H), 5.18 (d, *J* = 3.9 Hz, 1H), 4.86 (d, *J* = 9.1 Hz, 3H), 4.51 (s, 2H), 3.90 (q, *J* = 7.0 Hz, 1H), 3.76 (s, 3H), 3.60 (dq, *J* = 12.0, 6.0 Hz, 1H), 3.45 – 3.36 (m, 2H), 2.84 – 2.74 (m, 2H), 2.46 (d, *J* = 30.8 Hz, 1H), 1.87 (dd, *J* = 14.7, 4.3 Hz, 1H), 1.67 (dt, *J* = 13.1, 6.6 Hz, 1H), 1.53 (dd, *J* = 13.3, 4.9 Hz, 1H), 1.02 (d, *J* = 6.4 Hz, 3H). ^{13}C NMR (101 MHz, $CDCl_3$) δ 213.81, 186.36, 162.47, 135.64, 119.47, 118.52, 100.77, 76.31, 69.37, 68.83, 67.45, 65.24, 56.49, 53.46, 47.24, 36.32, 35.61, 33.43, 31.21, 29.84, 16.74. HRMS (ESI^-) m/z: calculated for $C_{35}H_{29}F_4N_4O_{13}$ ($[M-H]^-$): 789.1672; found: 789.1668.

1.4 General synthetic route of sulfonyl azide-motif compound 8

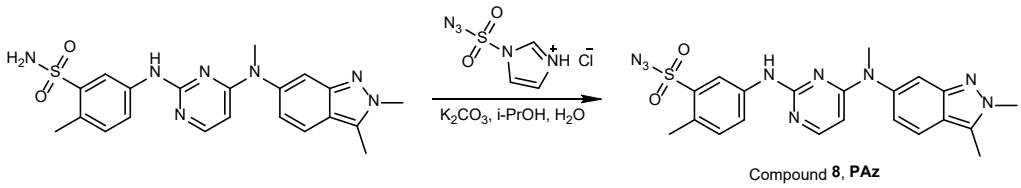

Scheme S5. Synthetic route of compound 8.

Compound **8** was synthesized following previously reported procedures and the characterization matched with the previously reported data[1].

1.5 General synthetic route of boronic acid/boronate-motif compound 11

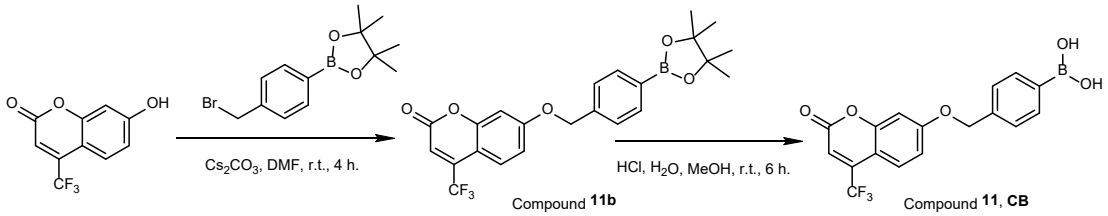

Scheme S6. Synthetic route of compound 11.

4-(Bromomethyl)phenylboronic acid pinacol ester (41 mg, 0.13 mmol) and 7-hydroxy-4-(trifluoromethyl)coumarin (30 mg, 0.13 mmol) were dissolved in DMF (5 mL), followed by the addition of Cs_2CO_3 (46 mg, 0.14 mmol). The mixture was stirred at room temperature for 4 h and then quenched with saturated $NaHCO_3$ solution. The mixture was extracted with ethyl acetate (3 × 20 mL), washed, dried over anhydrous $MgSO_4$, filtered, and concentrated under reduced pressure. The crude product was

purified by flash chromatography (cyclohexane/EtOAc = 100:0 to 60:40, v/v) to give compound **11b** (35 mg, 60% yield, white solid). Then **11b** (30 mg, 0.067 mmol) was dissolved in a mixture of methanol and water (10 mL, v/v = 3:1). The solution was acidified to pH 2 by dropwise addition of 1 M HCl and stirred at room temperature for 6 h. The reaction mixture was then neutralized with saturated $NaHCO_3$ solution. After removal of organic solvents under reduced pressure, the resulting precipitate was collected by filtration, washed, and dried to afford compound **11**. ^{1}H NMR (400 MHz, DMSO-d_6) δ 7.72 (d, J = 7.7 Hz, 2H), 7.63 (dd, J = 9.2, 2.1 Hz, 1H), 7.49 (d, J = 7.6 Hz, 2H), 7.22 (d, J = 2.4 Hz, 1H), 7.14 (dd, J = 9.0, 2.5 Hz, 1H), 6.86 (s, 1H), 5.32 (s, 2H), 1.30 (s, 12H). ^{13}C NMR (101 MHz, DMSO-d_6) δ 162.42, 159.14, 156.24, 139.83, 135.12, 135.04, 127.74, 127.45, 126.35, 114.44, 113.91, 107.11, 103.10, 84.19, 70.27, 40.63, 40.47, 40.27, 25.14.

1.6 General synthetic route of α-ketoamide-motif compound 15

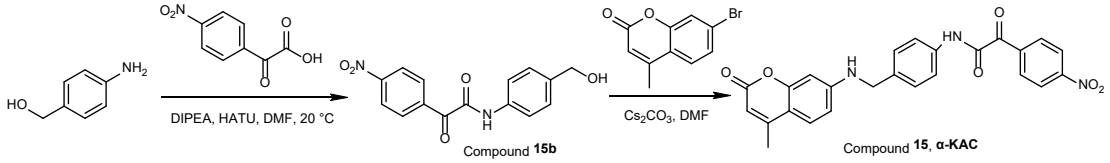

Scheme S7. Synthetic route of compound 15.

(4-aminophenyl)methanol (61.6 mg, 0.5 mmol) was dissolved in DMF (5 mL), followed by the addition of DIPEA (120 μL, 0.7 mmol) and HATU (245 mg, 0.6 mmol). The mixture was stirred for 15 min, after which 4-nitrophenylglyoxylic acid (117 mg, 0.6 mmol) was added. The mixture was stirred at room temperature for 2 h. Upon completion, the reaction was quenched, and the mixture was extracted with ethyl acetate (3 × 20 mL), dried over anhydrous $MgSO_4$, filtered, and concentrated under reduced pressure to afford **15b** (150 mg, 96% yield). The above intermediate (90 mg, 0.3 mmol) and 7-bromo-4-methylcoumarin (95 mg, 0.4 mmol) were dissolved in DMF (5 mL), followed by the addition of Cs_2CO_3 (1.17 g, 3.6 mmol). The mixture was stirred for 12 h and then the reaction was quenched, and filtered and extracted with ethyl acetate (3 × 20 mL), dried over anhydrous $MgSO_4$, and concentrated under reduced pressure. The crude product was purified by flash chromatography (PE/EA = 50:10 to 20:10, v/v) to give compound **15** (96 mg, 70% yield, white solid).

1.7 General synthetic route of pentafluorobenzenesulfonyl ester-motif compound 16

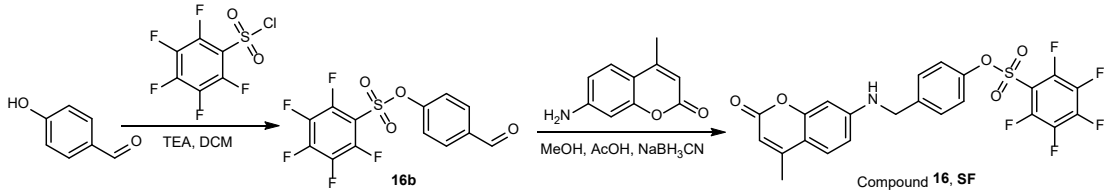

Scheme S8. Synthetic route of compound 16.

4-Hydroxybenzaldehyde (12.2 mg, 0.1 mmol) was dissolved in DCM (5 mL), followed by the addition of pentafluorobenzenesulfonyl chloride (31.9 mg, 0.12 mmol) and triethylamine (TEA, 20.9 μL, 0.15 mmol). The mixture was stirred at room temperature for 2 h. Upon completion, the reaction was quenched, dried over anhydrous $MgSO_4$, filtered, and concentrated under reduced pressure to afford **16b** (33.4 mg, 95% yield). Then **16b** was dissolved in DMF (5 mL), followed by the addition of 7-amino-4-methylcoumarin (17.5 mg, 0.1 mmol), sodium cyanoborohydride ($NaBH_3CN$, 6.5 mg, 0.1 mmol), and acetic acid (AcOH, 5 μL, 0.1 mmol). The reaction mixture was stirred overnight. Upon completion, the reaction was quenched, dried and concentrated under reduced pressure. The crude product was purified by flash chromatography (PE/EA = 10:1 to 5:1, v/v, gradient elution) to afford product **16** (46.1 mg, 95% yield, white solid).

1.8 General synthetic route of boronic acid/boronate-motif compounds 18−20

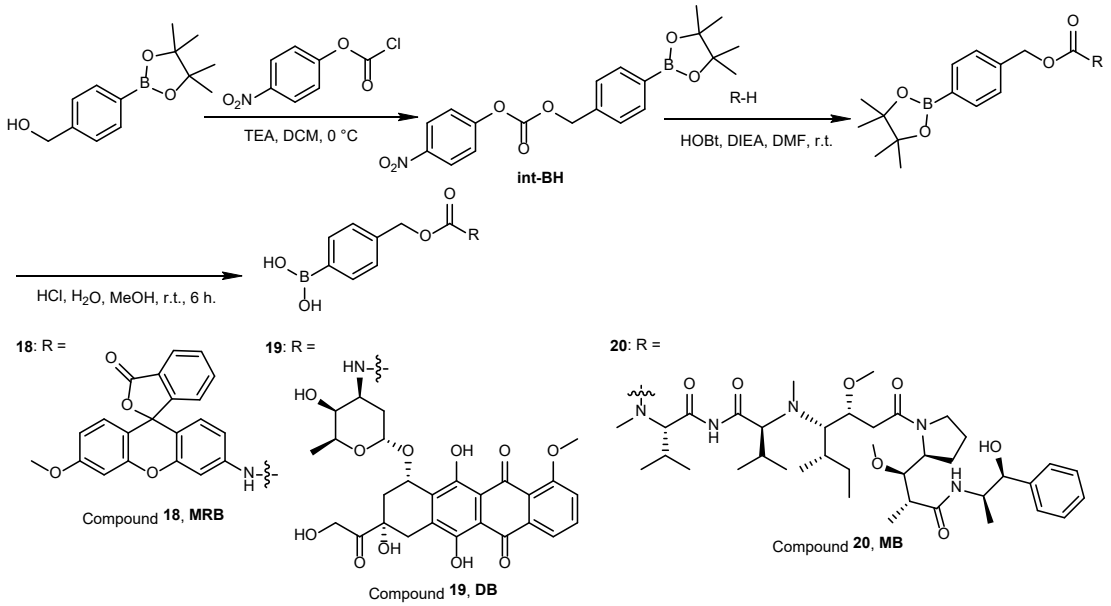

Scheme S9. General synthetic route of compounds 18−20.

4-Nitrophenyl chloroformate (264 mg, 1.26 mmol) was dissolved in dichloromethane (DCM, 3 mL) under an ice–water bath. TEA (177 μL, 1.26 mmol) was added dropwise, and the mixture was stirred under an argon atmosphere for 20 min. A solution of 4-(hydroxymethyl)phenylboronic acid pinacol ester (100 mg, 0.42 mmol) in DCM (4 mL) was then added dropwise, and the mixture was stirred at room temperature for 3 h. Then the reaction was quenched and extracted with DCM (3 × 20 mL), dried over anhydrous $MgSO_4$, filtered, and concentrated under reduced pressure. The crude product was purified by flash chromatography (cyclohexane/EtOAc = 90:10 to 60:40, v/v) to give the desired intermediate **int-BH** (135 mg, 80% yield, white solid). ^{1}H NMR (400 MHz, $CDCl_3$) δ 7.82 (dd, *J* = 7.7, 5.9 Hz, 2H), 7.69 – 7.54 (m, 2H), 7.43 – 7.33 (m, 2H), 6.77 – 6.60 (m, 2H), 3.84 (s, 2H), 1.34 (s, 12H).

The corresponding precursor (1 eq.) was dissolved in DMF (1 mL), and TEA (1 eq.) was added. The mixture was stirred at room temperature for 30 min, followed by the addition of HOBt (1 eq.) and a solution of **int-BH** (1 eq.) in DMF (1 mL). Upon completion, the reaction was quenched and dried over anhydrous $MgSO_4$, filtered, and concentrated under reduced pressure. The crude product was purified by flash chromatography to give the desired boronate ester-caged compound.

The boronate ester caged-compound was dissolved in a mixture of methanol and water (v/v = 3:1). The solution was acidified to pH 2 by dropwise addition of 1 M HCl and stirred at room temperature for 6 h. The reaction mixture was then neutralized with saturated $NaHCO_3$ solution. After removal of organic solvents under reduced pressure, the resulting precipitate was collected by filtration, washed, and dried to afford the desired boronic acid-caged compound.

Compound **18** (yellow solid): ^{1}H NMR (400 MHz, $CDCl_3$) δ 8.02 (dt, *J* = 7.3, 1.2 Hz, 1H), 7.84 – 7.78 (m, 1H), 7.64 (dtd, *J* = 20.4, 7.4, 1.2 Hz, 2H), 7.55 (s, 1H), 7.38 (d, *J* = 7.8 Hz, 1H), 7.15 (dt, *J* = 7.6, 1.0 Hz, 1H), 6.90 (dd, *J* = 8.6, 2.2 Hz, 1H), 6.89 – 6.76 (m, 2H), 6.75 (s, 1H), 6.74 – 6.65 (m, 2H), 6.61 (dd, *J* = 8.8, 2.5 Hz, 1H), 3.84 (s, 3H), 3.80 (s, 3H), 1.41 – 1.15 (m, 12H).

Compound **19** (red solid): ^{1}H NMR (400 MHz, DMSO-d_6) δ 13.92 (d, *J* = 3.3 Hz, 1H), 13.16 (s, 1H), 7.77 (dq, *J* = 16.3, 8.1 Hz, 2H), 7.60 (d, *J* = 7.5 Hz, 2H), 7.51 (d, *J* = 8.1 Hz, 1H), 7.29 (d, *J* = 7.6 Hz, 2H), 6.95 (d, *J* = 7.9 Hz, 1H), 5.39 (s, 1H), 5.21 (d, *J* = 3.6 Hz, 1H), 5.04 – 4.92 (m, 2H), 4.88 (t, *J* = 6.0 Hz, 2H), 4.74 (d, *J* = 5.7 Hz, 1H), 4.60 (d, *J* = 5.9 Hz, 2H), 4.18 (q, *J* = 6.7 Hz, 1H), 3.92 (s, 3H),

3.80 – 3.69 (m, 1H), 3.50 – 3.44 (m, 1H), 2.99 – 2.79 (m, 2H), 2.22 (d, J = 14.2 Hz, 1H), 2.07 (q, J = 5.6 Hz, 1H), 1.88 (td, J = 12.9, 3.7 Hz, 1H), 1.50 (dd, J = 12.4, 4.5 Hz, 1H), 1.30 (d, J = 3.8 Hz, 1H), 1.25 (s, 10H), 1.22 (s, 1H), 1.15 (d, J = 6.4 Hz, 3H), 1.08 (s, 2H). ^{13}C NMR (101 MHz, DMSO-d_6) δ 214.35, 186.66, 186.51, 161.10, 156.53, 155.69, 154.93, 141.00, 136.51, 135.80, 134.86, 134.56, 134.39, 127.14, 126.94, 120.15, 119.94, 119.28, 111.00, 110.88, 100.85, 84.07, 75.37, 74.00, 70.25, 68.45, 67.13, 65.31, 64.22, 56.91, 47.67, 36.86, 32.45, 30.28, 25.42, 25.08, 17.50.

Compound **20** (white solid): ^{1}H NMR (400 MHz, CD_3OD_SPE) δ 7.95 (dd, J = 31.4, 8.9 Hz, 1H), 7.75 (dd, J = 10.0, 4.9 Hz, 1H), 7.67 – 7.59 (m, 1H), 7.46 – 7.25 (m, 7H), 7.22 (td, J = 8.9, 5.4 Hz, 1H), 5.25 (dt, J = 11.0, 5.6 Hz, 1H), 4.59 (dd, J = 20.8, 6.9 Hz, 2H), 4.33 – 4.16 (m, 3H), 3.77 – 3.51 (m, 2H), 3.46 – 3.34 (m, 6H), 3.32 (s, 2H), 3.29 (s, 2H), 3.13 (s, 2H), 2.98 (d, J = 10.7 Hz, 4H), 2.54 – 2.47 (m, 2H), 2.33 – 2.12 (m, 3H), 2.11 – 1.68 (m, 7H), 1.59 (dddt, J = 14.9, 11.4, 7.5, 3.3 Hz, 3H), 1.50 – 1.40 (m, 2H), 1.40 – 1.31 (m, 4H), 1.31 (d, J = 3.6 Hz, 4H), 1.23 – 1.11 (m, 8H), 1.11 – 0.76 (m, 28H). ^{13}C NMR (101 MHz, CD_3OD_SPE) δ 173.73, 157.40, 138.60, 138.15, 133.80, 133.44, 128.13, 127.85, 127.18, 127.05, 126.89, 126.65, 126.38, 85.31, 82.07, 78.32, 77.48, 76.07, 67.12, 64.56, 60.62, 60.23, 59.37, 59.21, 57.26, 56.93, 56.38, 54.94, 49.81, 47.76, 47.45, 47.24, 47.02, 46.69, 36.73, 35.35, 32.49, 32.27, 31.70, 30.57, 30.49, 29.40, 29.25, 28.95, 25.59, 25.24, 24.51, 24.16, 23.10, 18.38, 18.02, 17.69, 17.47, 15.47, 14.98, 14.60, 14.47, 13.92, 9.53.

1.9 General synthetic route of boronic acid-caged payload 21 and BSA conjugate 22

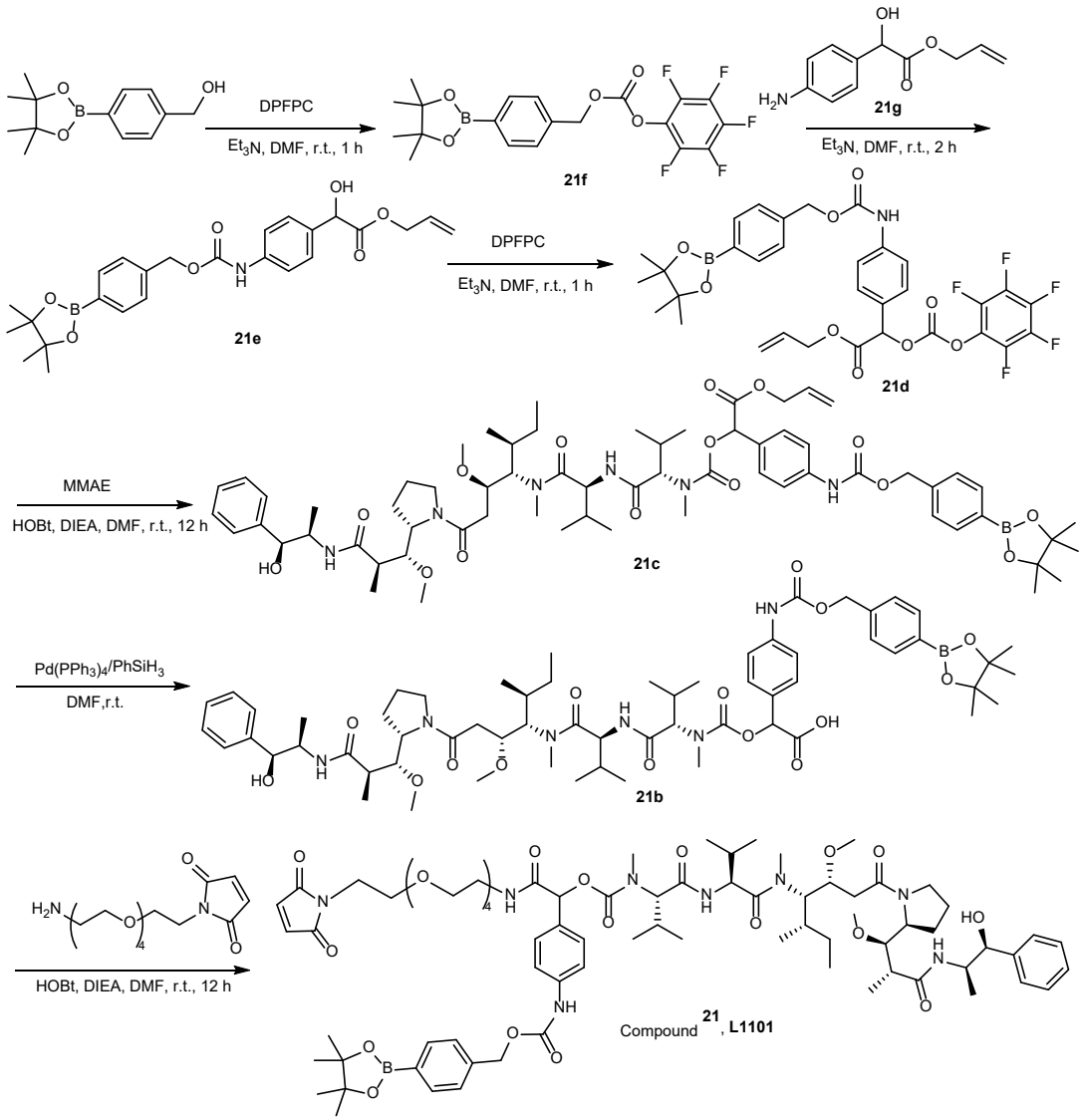

Scheme S10. General synthetic route of compound 21.

4-(Hydroxymethyl)phenylboronic acid pinacol ester (1.0 g, 4.27 mmol) was dissolved in DMF, followed by the addition of TEA (610 μL, 4.3 mmol) and dipentafluorophenyl carbonate (DPFPC, 1.7 g, 4.3 mmol). The mixture was stirred for 1 h and then purified by prep-HPLC to afford compound **21f** (1.7 g, 80% yield).

21f (1.0 g, 2.25 mmol) was dissolved in DMF, followed by the addition of TEA (320 μL, 2.3 mmol) and **21g** (0.47 g, 2.3 mmol). The mixture was stirred for 2 h and then purified by prep-HPLC to afford **21e** (0.65 g, 65% yield).

21e (1.2 g, 2.5 mmol) was dissolved in DMF, followed by the addition of TEA (350 μL, 2.5 mmol) and DPFPC (1.0 g, 2.5 mmol). The mixture was stirred for 1 h and then purified by prep-HPLC to afford **21d** (1.3 g, 80% yield).

21d (145 mg, 0.21 mmol) was dissolved in DMF, followed by the addition of MMAE (193 mg, 0.32 mmol) and HOBt (47 mg, 0.35 mmol) dissolved in DMF, as well as DIEA (120 μL, 0.68 mmol). The mixture was stirred at room temperature overnight and then purified by prep-HPLC to afford **21c** (140 mg, 60% yield).

21c (120 mg, 0.1 mmol) was dissolved in DMF, followed by the addition of $Pd(PPh_3)_4$ (11.6 mg, 0.01 mmol) and phenylsilane ($PhSiH_3$, 55 mg, 0.5 mmol). The reaction was carried out under an argon

atmosphere at room temperature for 2 h and then purified by prep-HPLC to afford **21b** (103 mg, 90% yield).

21b (144 mg, 0.12 mmol) was dissolved in DMF, followed by the addition of Mal-PEG4-amine TFA salt (52 mg, 0.12 mmol), HOBt (23 mg, 0.16 mmol), and DIEA 60 μL, 0.34 mmol). The reaction mixture was stirred at room temperature overnight and then purified by prep-HPLC to afford compound **21** (147 mg, 82% yield, white solid).

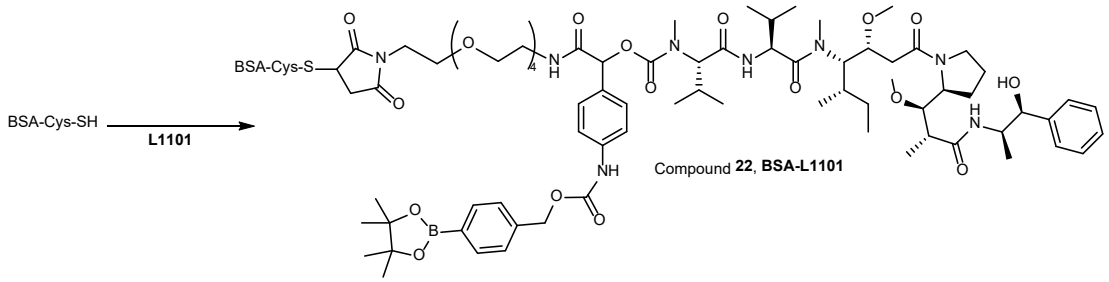

Scheme S11. General synthetic route of compound 22.

The above compound **21**, dissolved in DMSO, was added to a PBS (pH 7.4) solution containing bovine serum albumin (BSA, 1 mg/mL, 14.7 μM) to give a final concentration of 73.5 μM (5 eq.). The mixture was incubated at room temperature for 2 h. Subsequently, unreacted conjugate L1101 was removed by centrifugal ultrafiltration (30 kDa molecular weight cutoff) to afford BSA–L1101.

2. Supplementary Tables

Supplementary Tab. 1 | Proposed mechanistic schemes for ultrasound-triggered activation of DHBC and DMOBC-motifs.

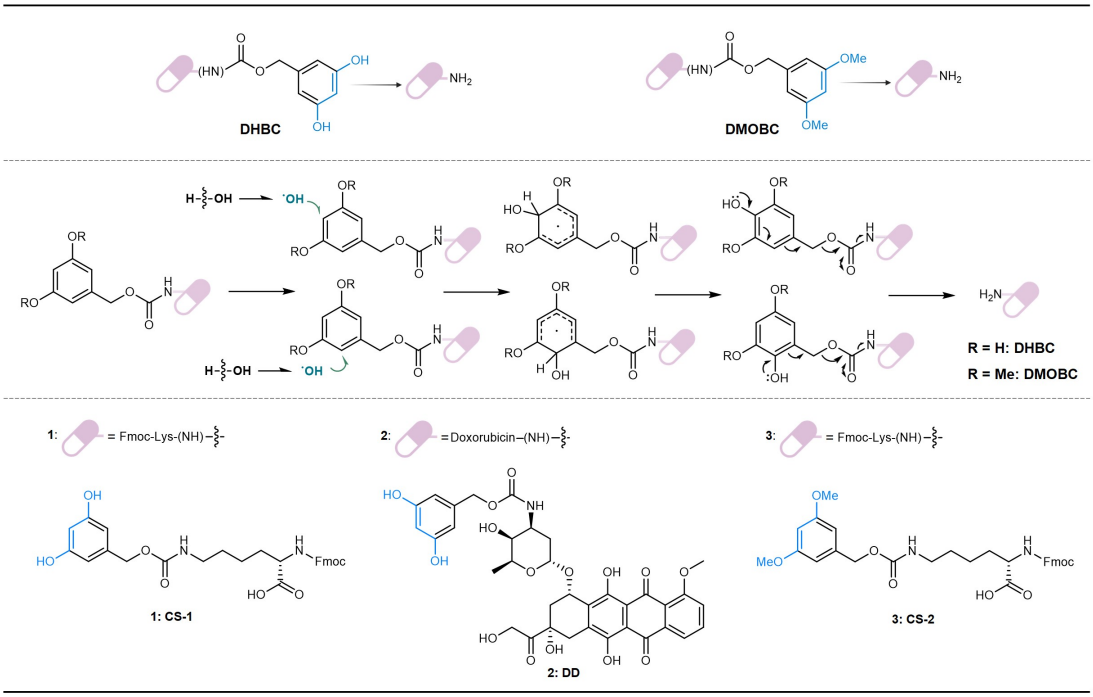

Supplementary Tab. 2 | Proposed mechanistic schemes for ultrasound-triggered activation of azide-motifs.

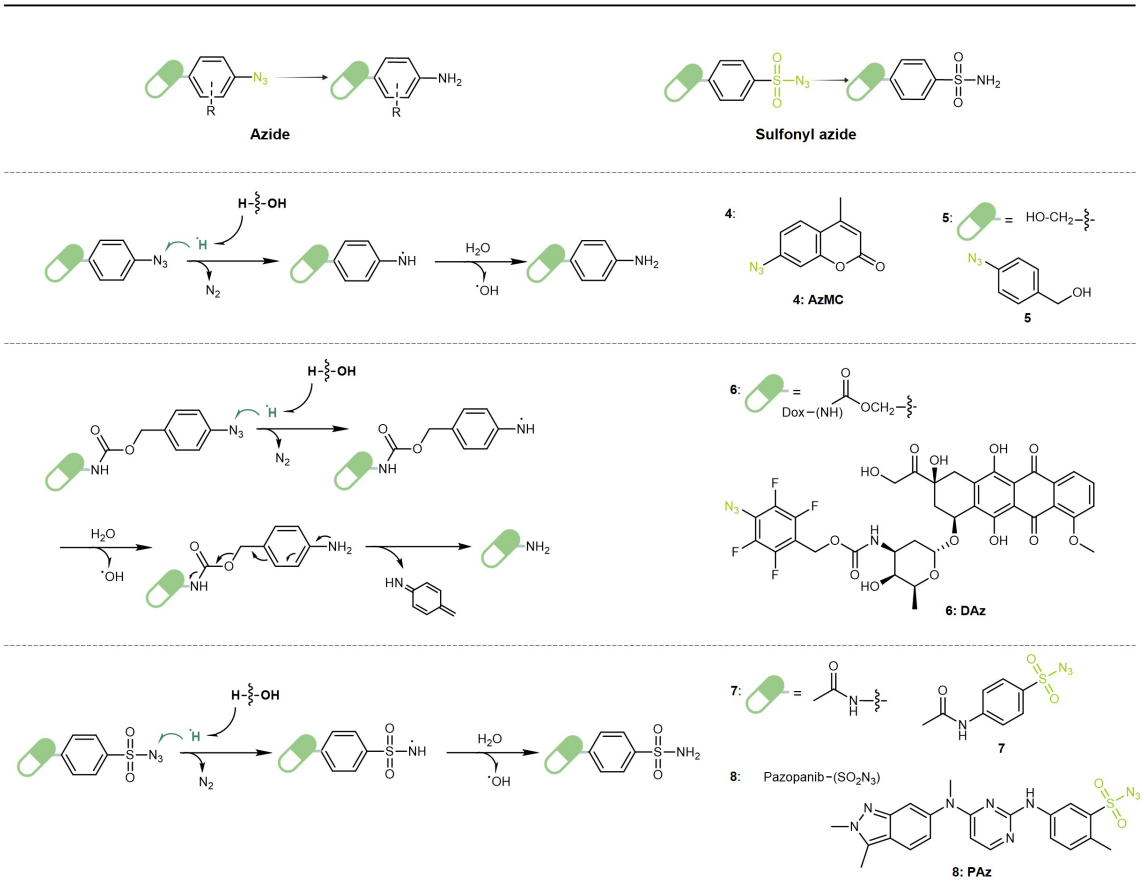

Supplementary Tab. 3 | Proposed mechanistic schemes for ultrasound-triggered activation of boronic acid/boronate -motifs.

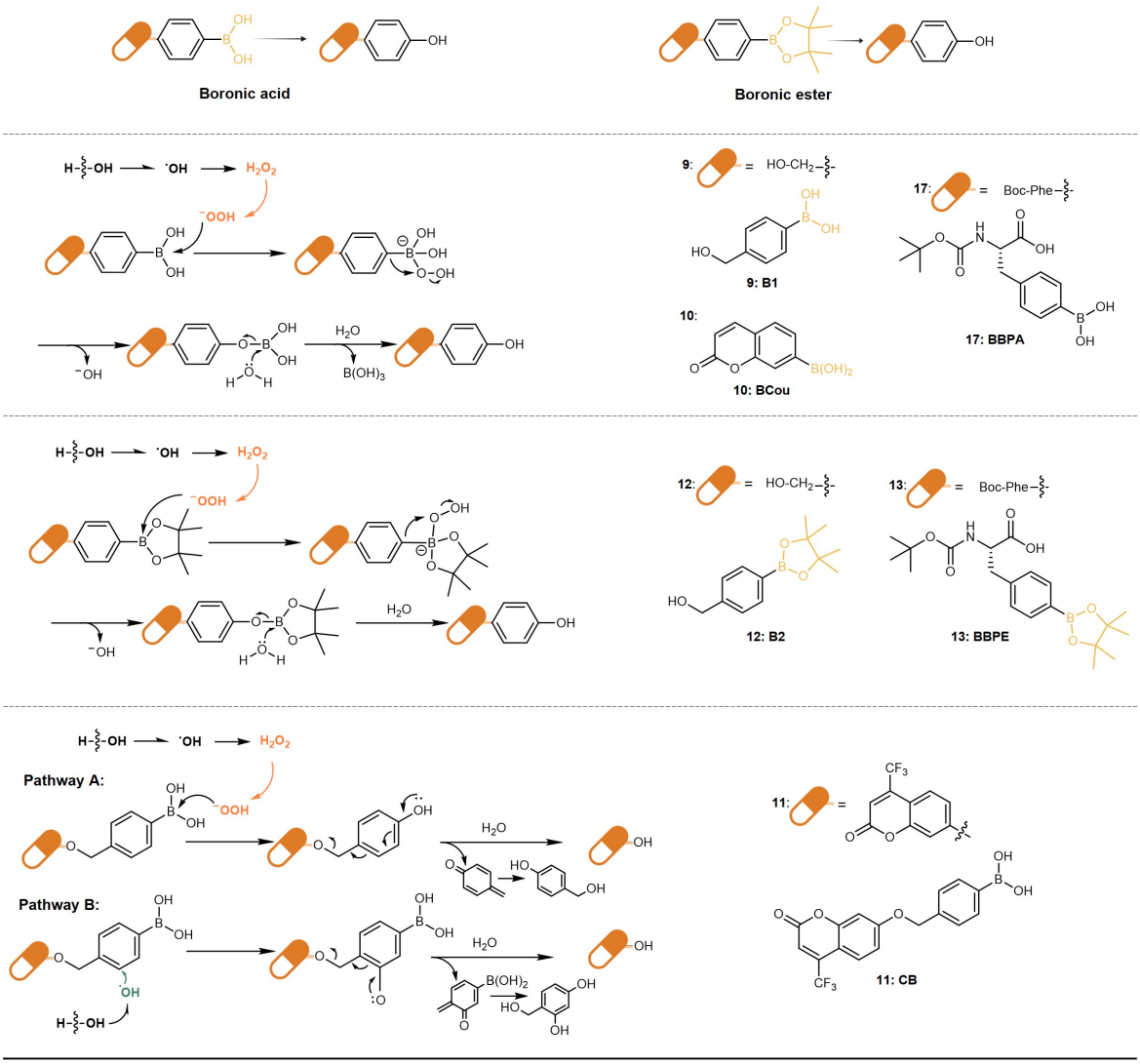

Supplementary Tab. 4 | Proposed mechanistic schemes for ultrasound-triggered activation of other peroxide-responsive motifs.

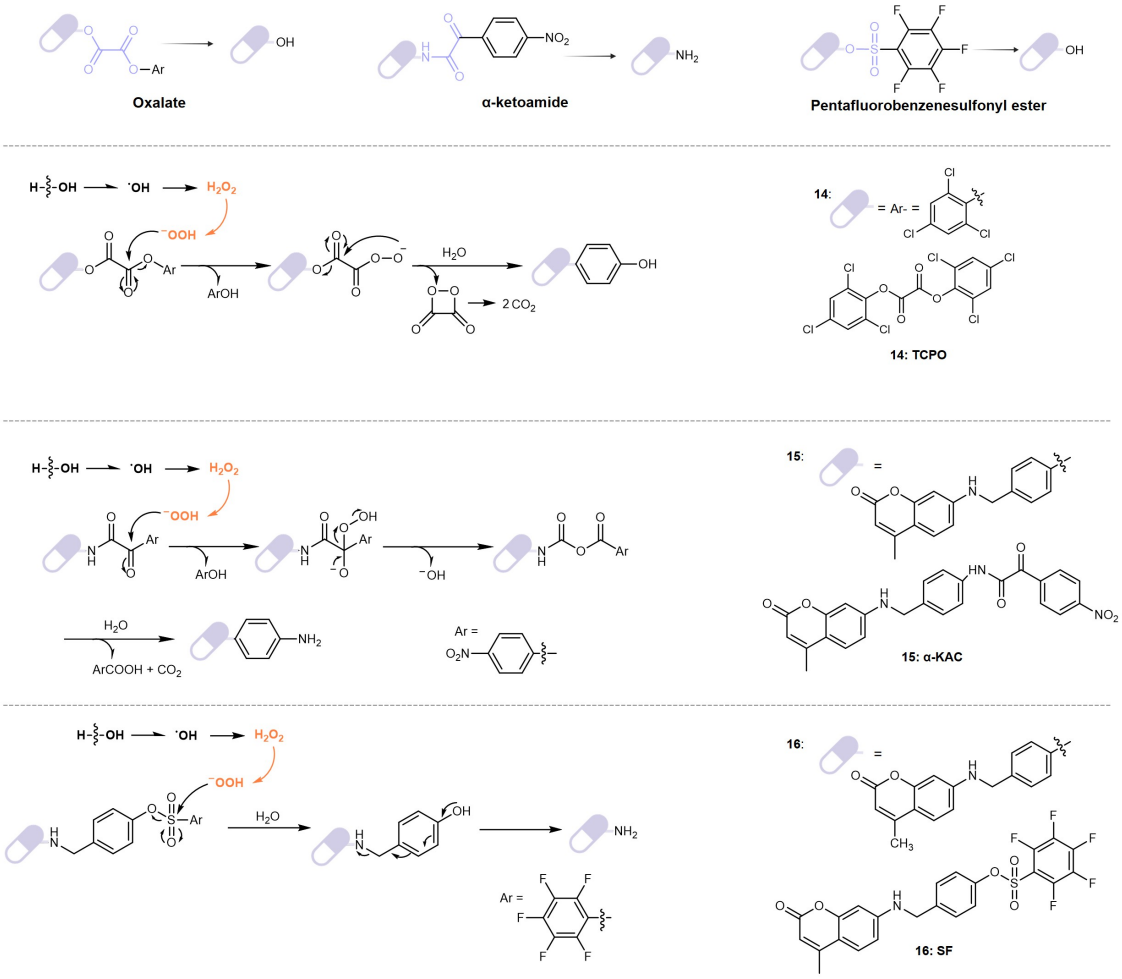

Supplementary Tab. 5 | Comparison of in vitro scavenging abilities of representative molecules toward hydroxyl radicals (•OH) and hydrogen peroxide (H_2O_2).

Molecule	In vitro scavenging ability toward •OH	In vitro scavenging ability toward H_2O_2	Main mechanism	Typical second-order rate constant with •OH (M^{-1} s^{-1})	Notes	Analysis
Glutathione (GSH)	Strong	Moderate	Thiol oxidation	~10^{10}	More efficient in the presence of enzymatic systems	Presence of GSH/NAC leads to decreased production of hydroxylated products (Bxs). NAC exhibits weaker H_2O_2 quenching capacity than GSH, thus exerting a lesser influence on the B1 deboronation reaction.
N-Acetylcysteine (NAC)	Strong	Weak–moderate	Thiol oxidation	~10^{9}	Mechanistically similar to GSH	
Vitamin E (VE)	Moderate	Negligible	Radical chain termination	~10^{8} (in lipid phase)	Mainly scavenges lipid peroxyl radicals	Despite being only a moderate hydroxyl radical quencher, experiments indicate that VE effectively quenches •OH generated from the interface of US-induced cavitation bubbles (B_xs production ↓↓).
5,5-Dimethyl-1-pyrroline N-oxide (DMPO)	Not a scavenger but a detection probe	Negligible	Spin trapping	~10^{9}	Used for EPR detection of radicals	DMPO inhibits H_2O_2 production by capturing •OH radicals.
Isopropanol (IPA)	Very strong	Negligible	Hydrogen abstraction reaction	~10^{9}	Standard hydroxyl radical scavenger in ROS studies	Experiments show that IPA scavenges •OH (hence B_xs production ↓), but induces H_2O_2 production (hence B_0 production ↑),

3. Supplementary Figures

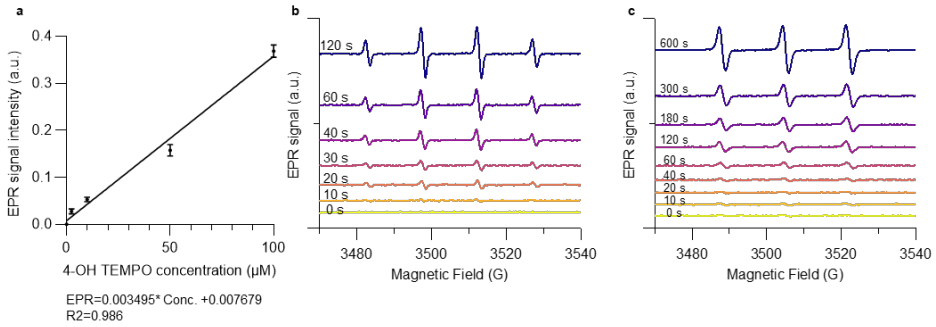

Supplementary Fig. 1 | Qualitative EPR characterization of reactive oxygen species generated during ultrasound irradiation.

Representative EPR spectra confirm the formation of ROS under ultrasound treatment (**b**, hydroxyl radical; **c**, singlet oxygen), supporting cavitation-driven water sonolysis as the chemical basis of sono-orthogonal activation.

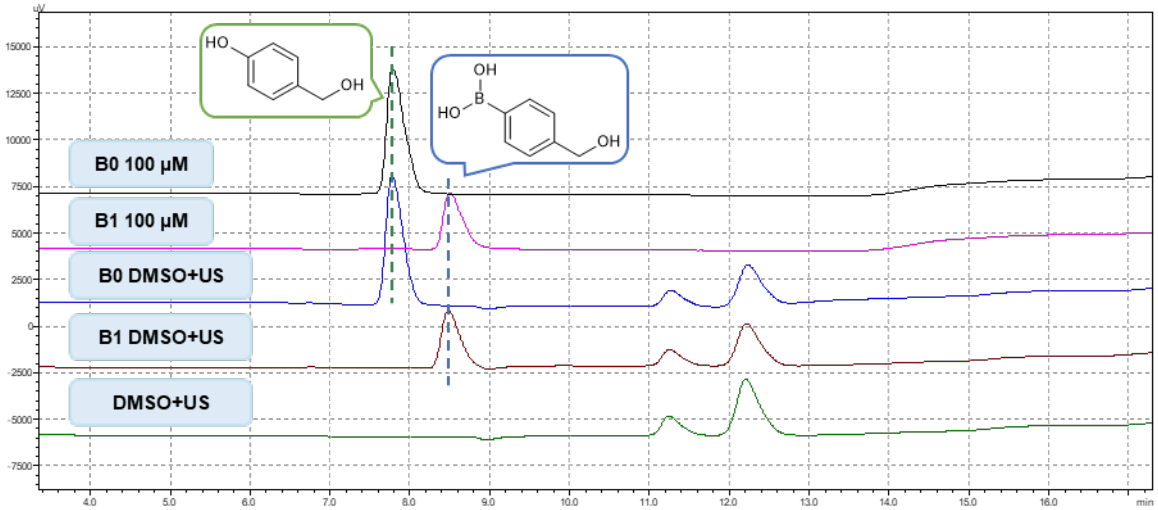

Supplementary Fig. 2 | HPLC analysis of ultrasound-triggered conversion of B1 to B0 and dependence on water participation.

HPLC analysis shows productive decaging of B1 under ultrasound in aqueous medium, whereas the absence of water in DMSO suppresses conversion, demonstrating that water-derived ROS are required for activation.

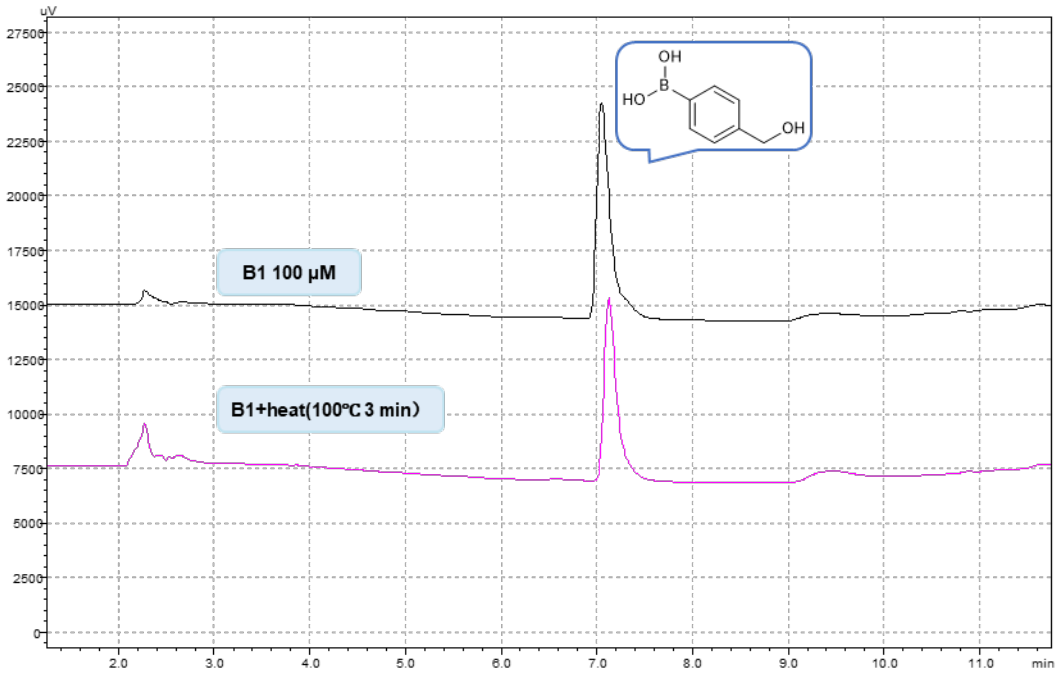

Supplementary Fig. 3 | HPLC analysis showing that ultrasound-triggered B1 decaging is not caused by thermal decomposition.

Control heating experiments do not reproduce the productive conversion observed under ultrasound, indicating that decaging is mechanochemical/sonochemical rather than thermally induced.

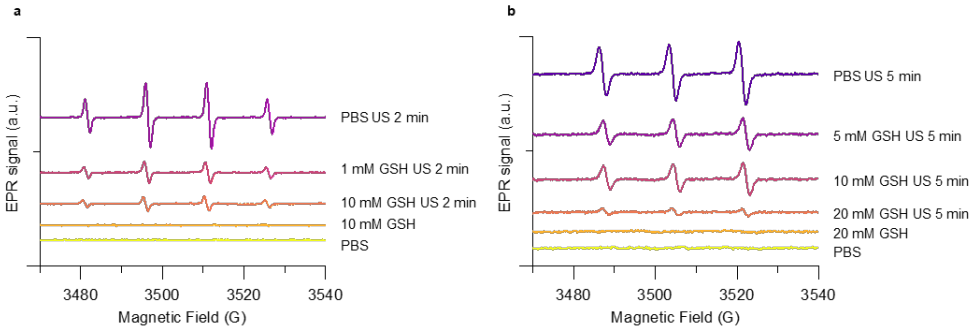

Supplementary Fig. 4 | EPR characterization of ultrasound-generated ROS under reductive conditions.

Representative spectra show that glutathione perturbs the generation of hydroxyl radicals and singlet oxygen under ultrasound, consistent with the sensitivity of transient interfacial radical chemistry to reductive environments.

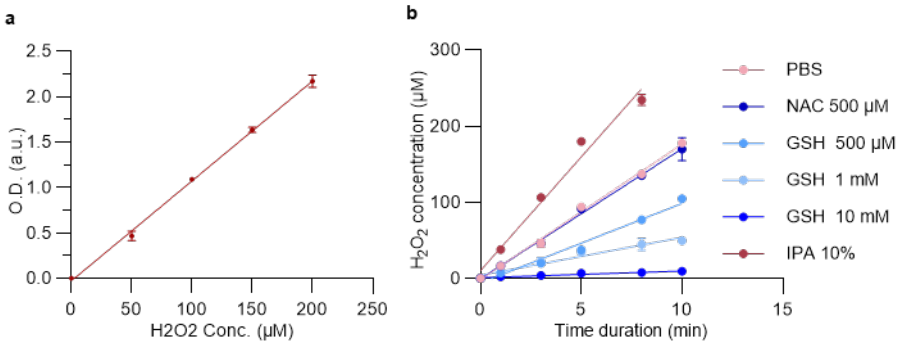

Supplementary Fig. 5 | Quantification of ultrasound-generated hydrogen peroxide by Amplex Red assay.

Hydrogen peroxide production during ultrasound irradiation was quantified in the presence of different additives. NAC minimally affects H_2O_2 formation, whereas GSH markedly suppresses it. IPA, despite being a ·OH radical quencher, unexpectedly promotes H_2O_2 accumulation, consistent with altered radical recombination pathways under ultrasound.

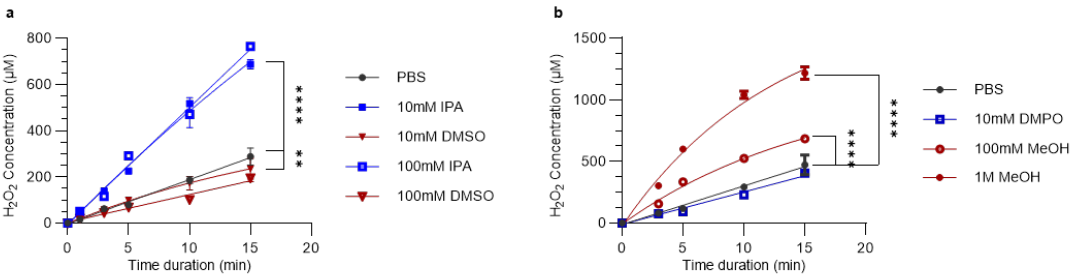

Supplementary Fig. 6 | Iodometric quantification of ultrasound-generated hydrogen peroxide under different reaction conditions.

Hydrogen peroxide formation was evaluated by iodometric analysis. IPA and MeOH increase H_2O_2 generation, whereas DMSO and DMPO suppress it.

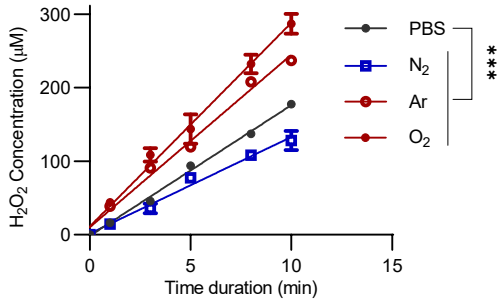

Supplementary Fig. 7 | Effects of gas atmosphere on hydrogen peroxide generation during ultrasound irradiation.

Amplex Red measurements show that O_2- and Ar-containing atmospheres promote H_2O_2 formation, whereas N_2 suppresses it.

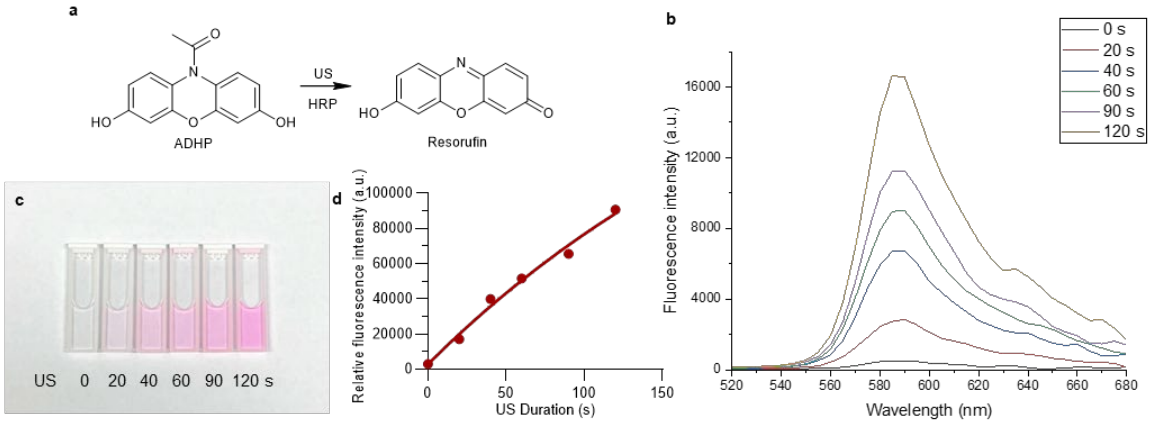

Supplementary Fig. 8 | Time dependence of the Amplex Red readout during ultrasound irradiation. The fluorescence of resorufin increases with ultrasound irradiation time, validating the time-dependent generation of hydrogen peroxide in the sonochemical system.

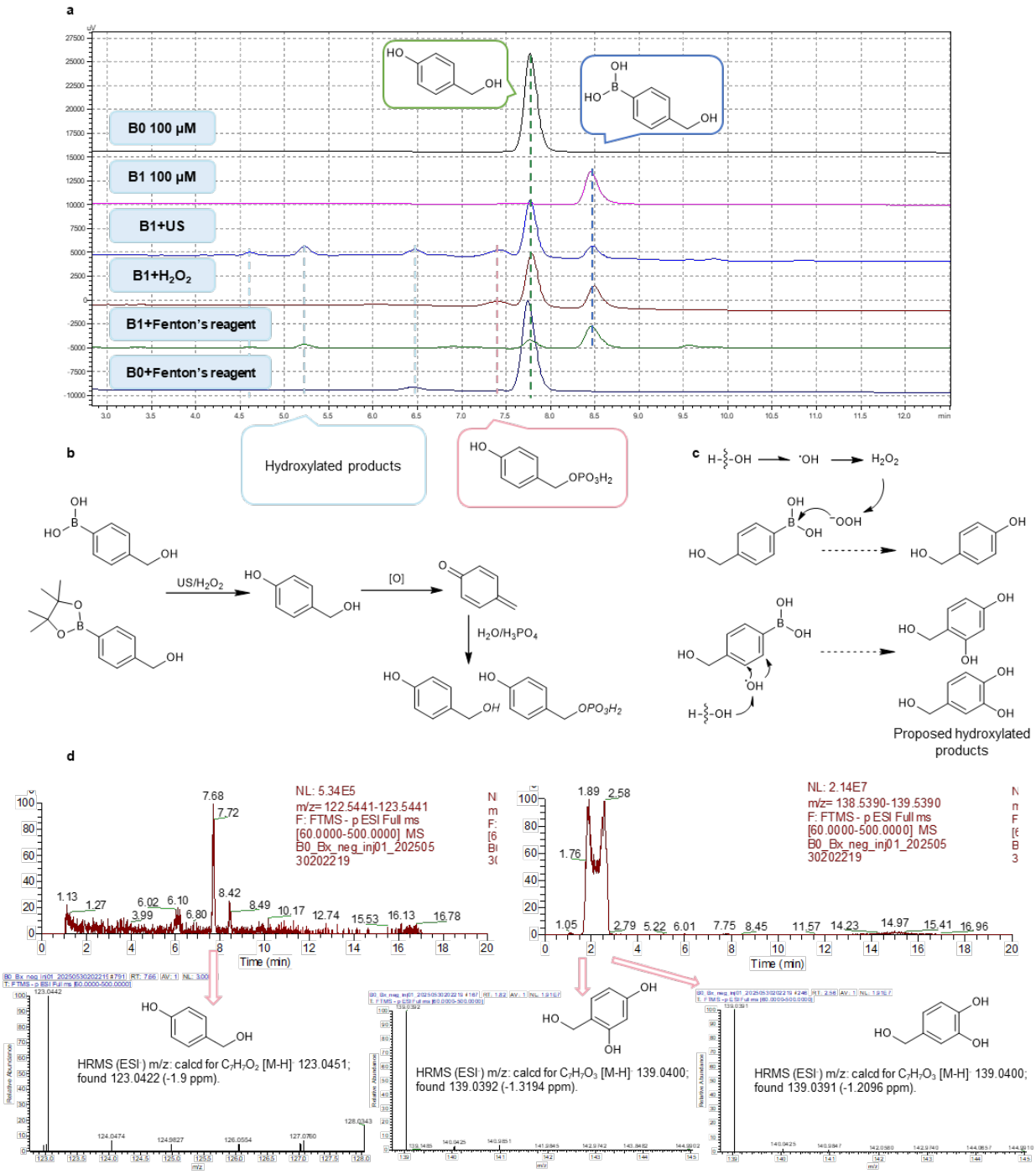

Supplementary Fig. 9 | Product analysis supporting dual-pathway boronic acid activation under ultrasound.

Both exogenous H_2O_2 and ultrasound convert B1 into B0 and the corresponding phosphorylated product, whereas ultrasound additionally produces the hydroxylated byproduct Bx. These data support a dominant persistent bulk activation pathway (1,6-elimination) accompanied by a minor transient interfacial activation pathway (1,4-elimination) under ultrasound. LC-MS characterization of B0 and Bx is shown in panel **d**.

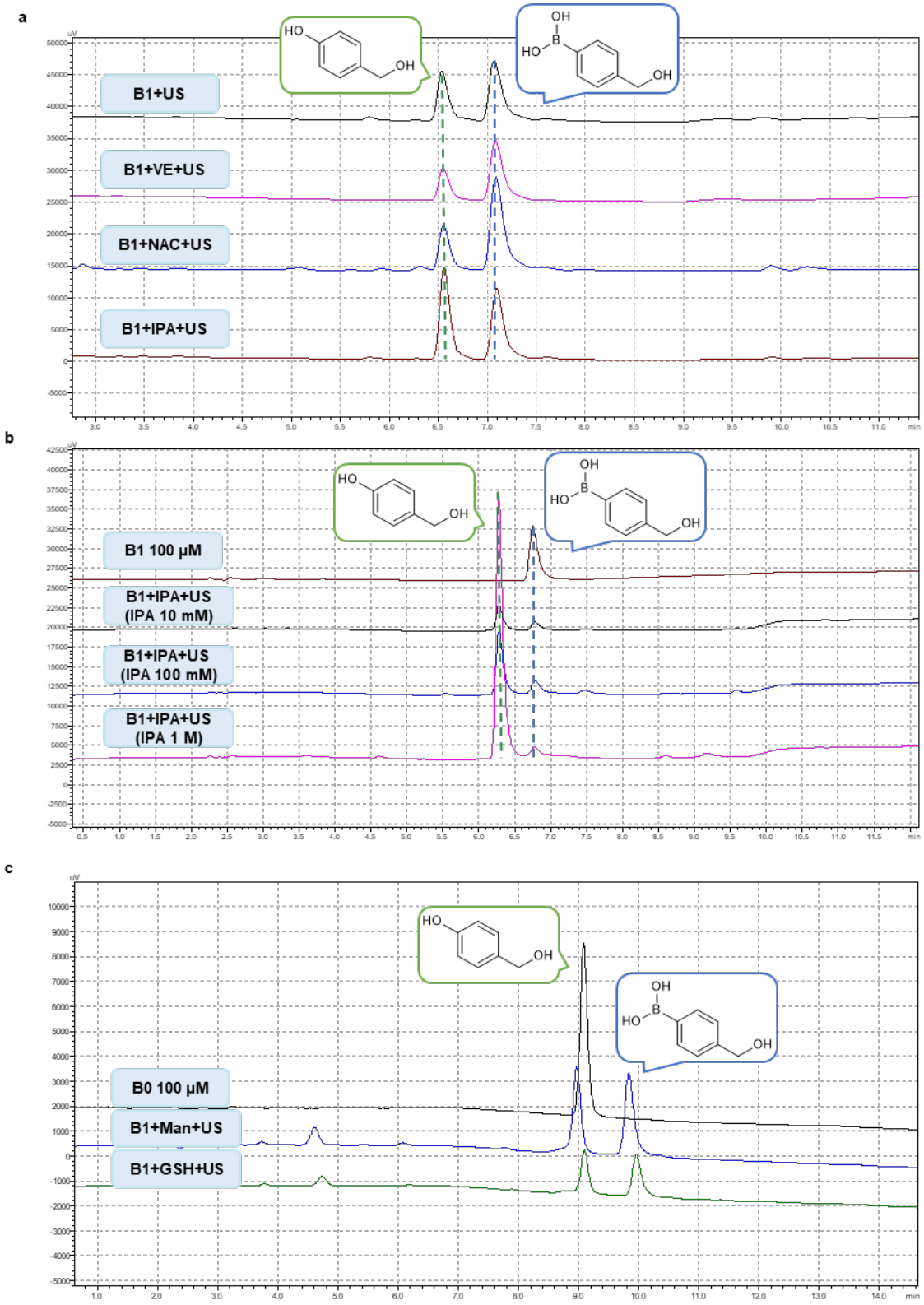

Supplementary Fig. 10 | HPLC analyses of B1 conversion in the presence of different scavengers. Selected scavengers differentially affect productive decaging and side-product formation. Hydroxyl-radical scavengers suppress Bx formation to varying extents. Lipophilic reductants such as VE strongly suppress B0 formation, suggesting efficient quenching of interfacial radical chemistry. IPA decreases Bx while promoting B0 formation, consistent with its ability to alter both radical scavenging and H_2O_2 accumulation.

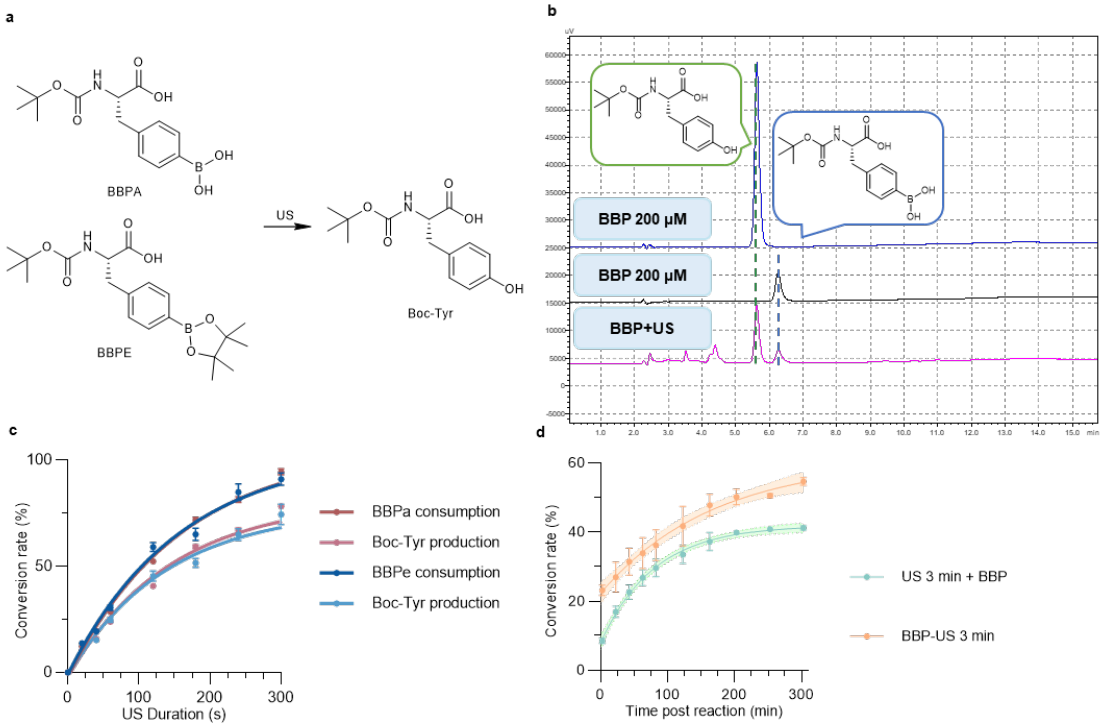

Supplementary Fig. 11 | Ultrasound-triggered activation of boronic acid/boronate-caged Boc-tyrosine derivatives.

Representative data show productive decaging of boronic acid/boronate-caged Boc-tyrosine derivatives under ultrasound. Comparison between direct ultrasound exposure and substrate addition after ultrasound pretreatment indicates that ultrasound contributes not only through persistent ROS generation but also through short-lived radical chemistry and accelerated reaction kinetics.

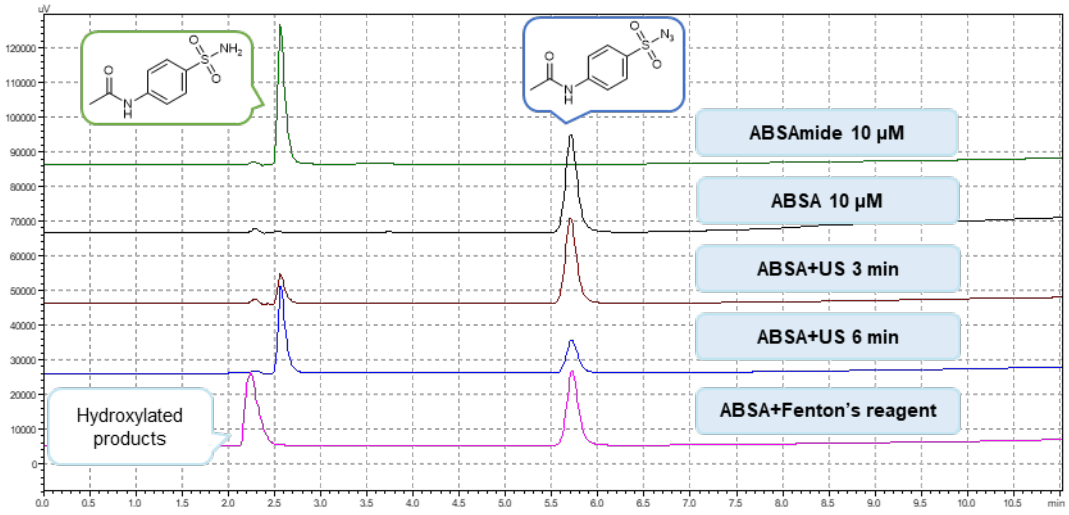

Supplementary Fig. 12 | Ultrasound-triggered conversion of the sulfonyl azide substrate ABSA.

ABSA is converted into the corresponding sulfonamide product under ultrasound, together with a minor hydroxylated byproduct.

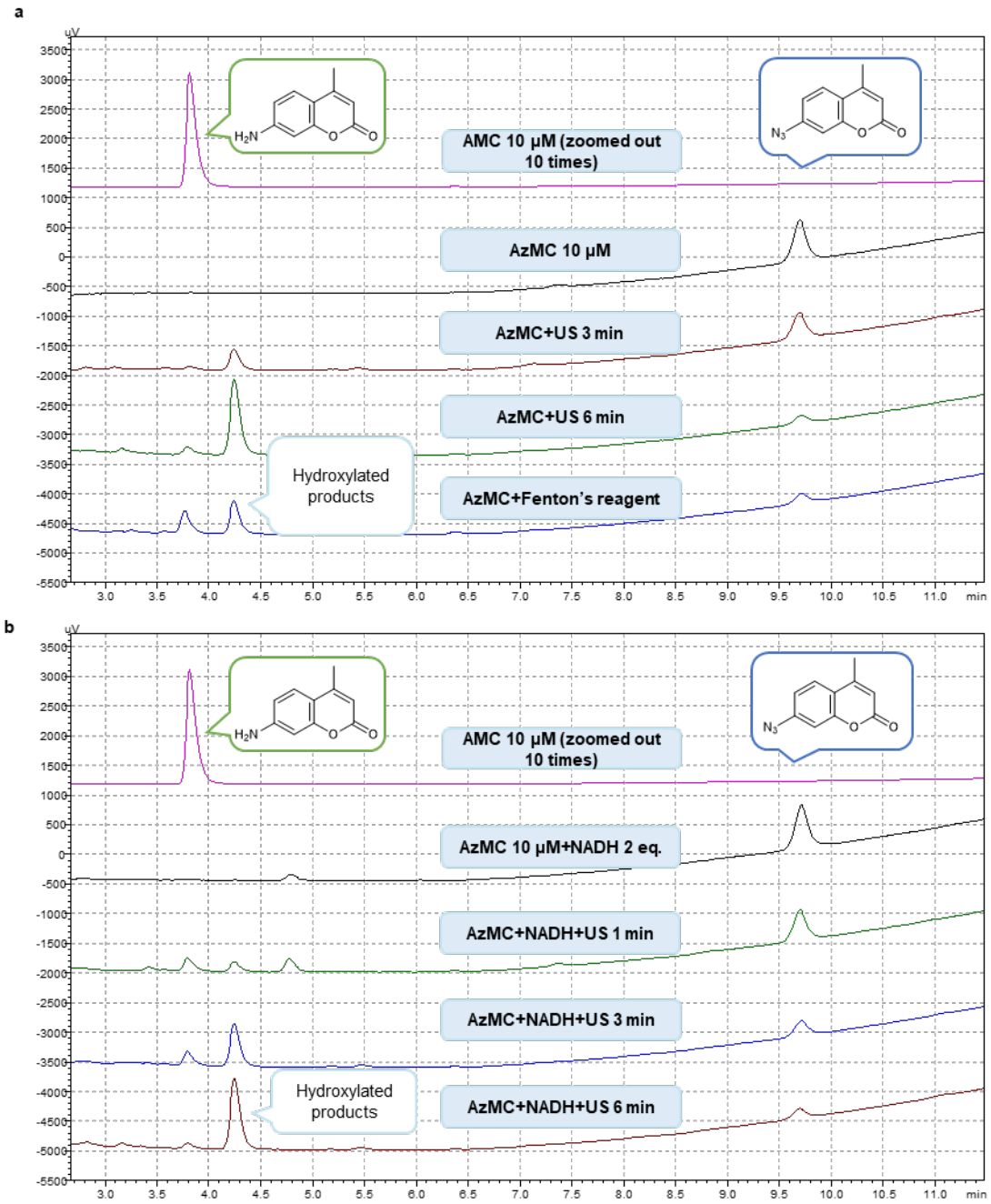

Supplementary Fig. 13 | Ultrasound-triggered conversion of the aryl azide substrate AzMC. AzMC is converted into AMC and hydroxylated byproducts under ultrasound. NADH promotes the productive transformation, supporting the distinct redox dependence of azide-based activation chemistry.

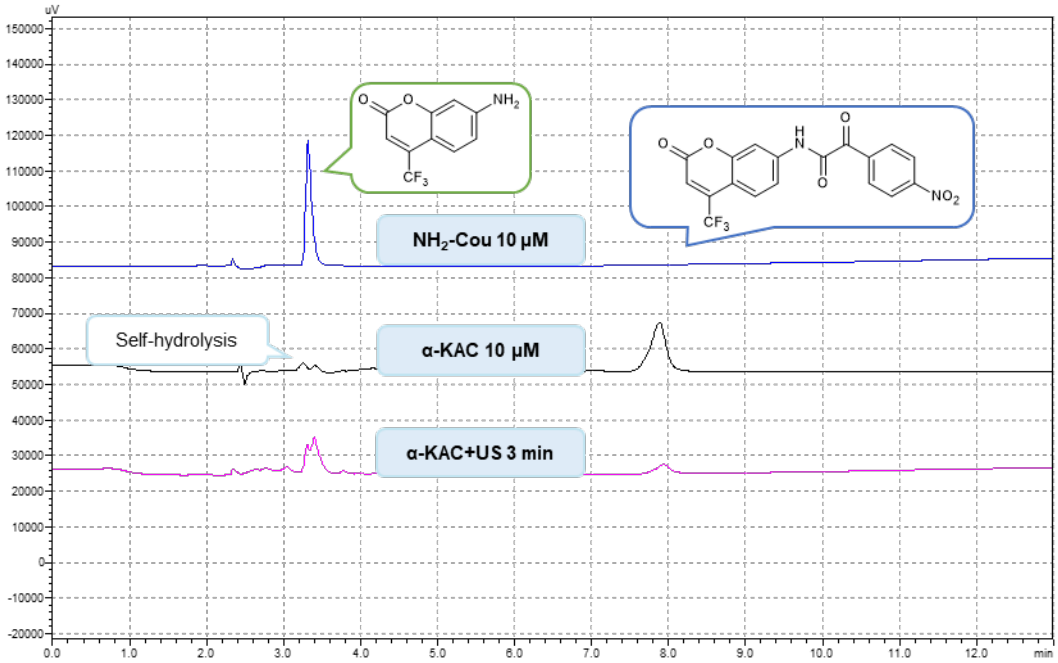

Supplementary Fig. 14 | Ultrasound-triggered conversion of the α-ketoamide substrate α-KAC. Representative chromatographic analyses show conversion of α-KAC into the corresponding amino-coumarin product under ultrasound irradiation.

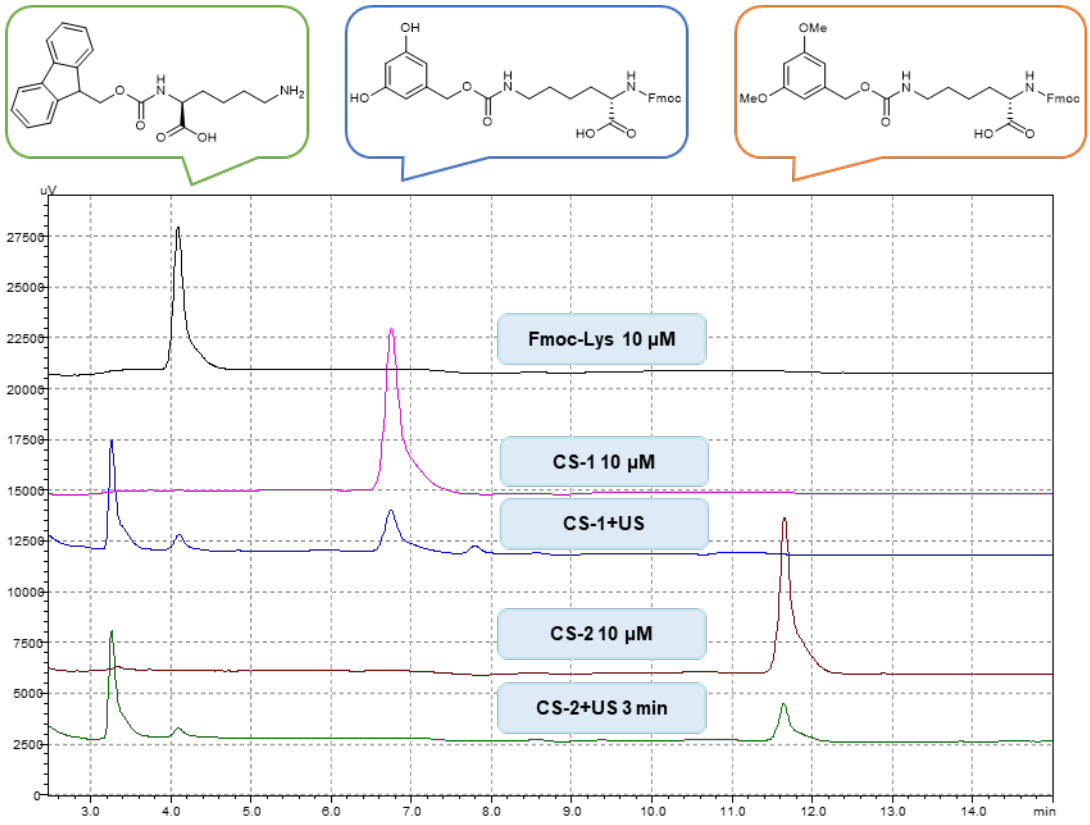

Supplementary Fig. 15 | Ultrasound-triggered activation of DHBC- and DMOBC-caged substrates. Representative data show conversion of CS-1 and CS-2 into Fmoc-Lys under ultrasound, supporting DHBC/DMOBC-type masking groups as transient interfacial activation motifs.

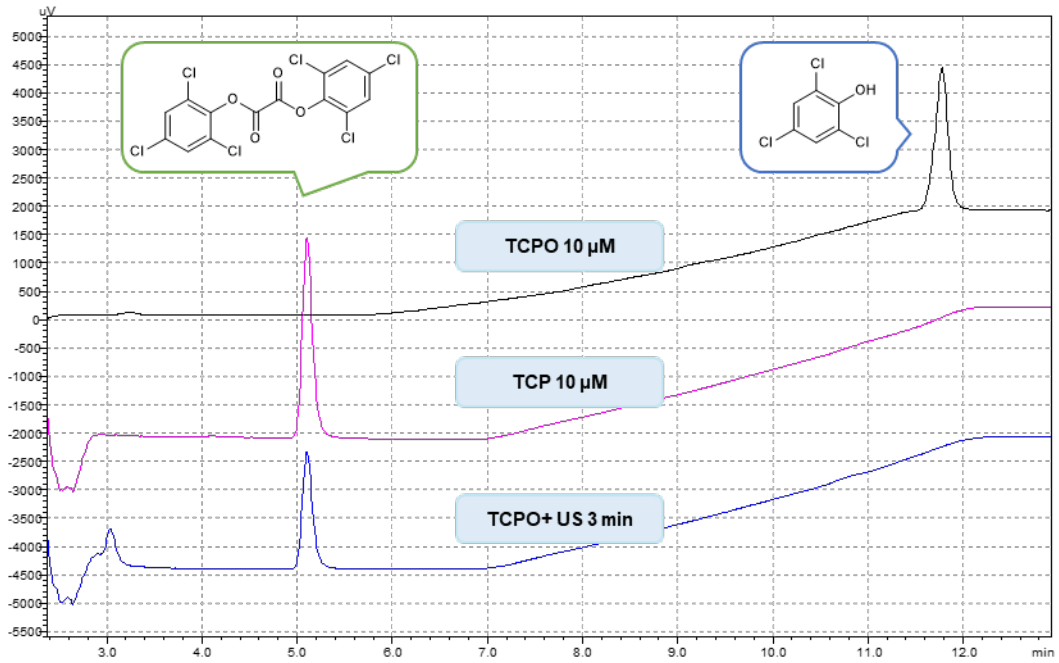

Supplementary Fig. 16 | Ultrasound-triggered conversion of the oxalate substrate TCPO.
TCPO undergoes ultrasound-triggered decomposition into TCP, illustrating the response of oxalate-based peroxide-sensitive motifs under the sonochemical conditions used here.

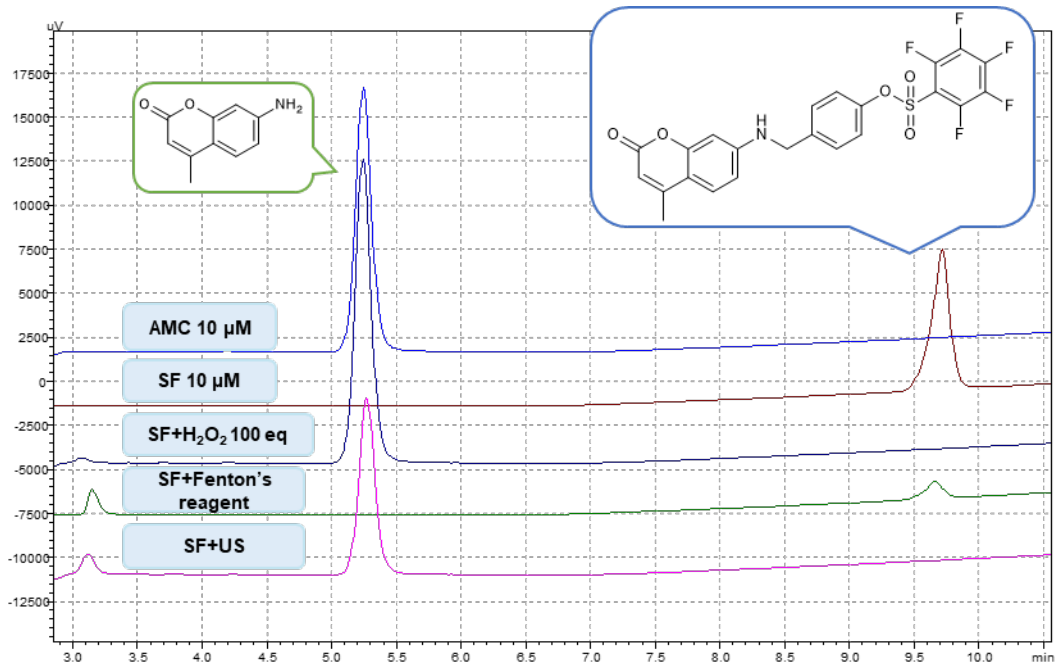

Supplementary Fig. 17 | Ultrasound-triggered conversion of the pentafluorobenzenesulfonyl ester substrate SF.
SF undergoes ultrasound-triggered decomposition into AMC, illustrating the response of pentafluorobenzenesulfonyl ester-based peroxide-sensitive motifs under the sonochemical conditions used here.

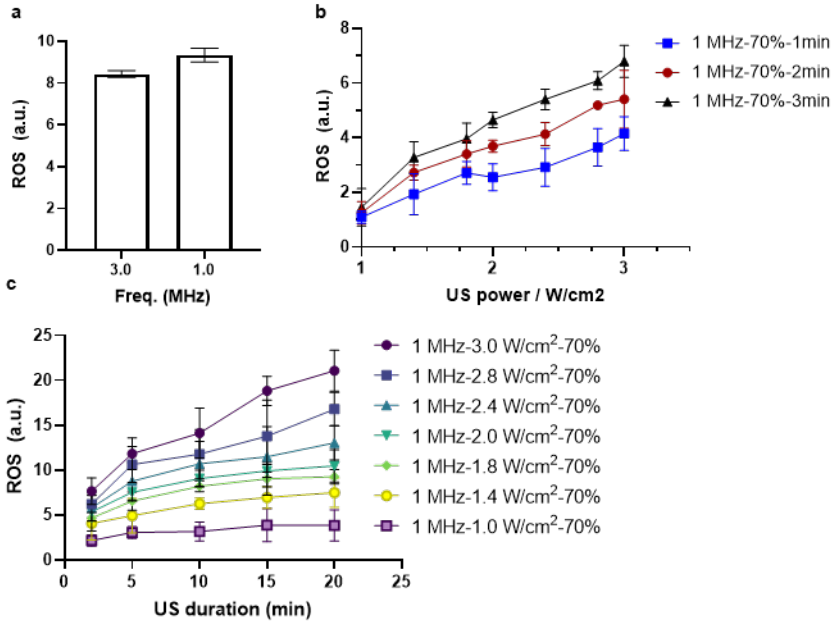

Supplementary Fig. 18 | Effects of ultrasound parameters on ROS generation measured by EPR. ROS production depends on ultrasound frequency, power, and irradiation time. Once cavitation is initiated, ROS output increases with power and irradiation duration.

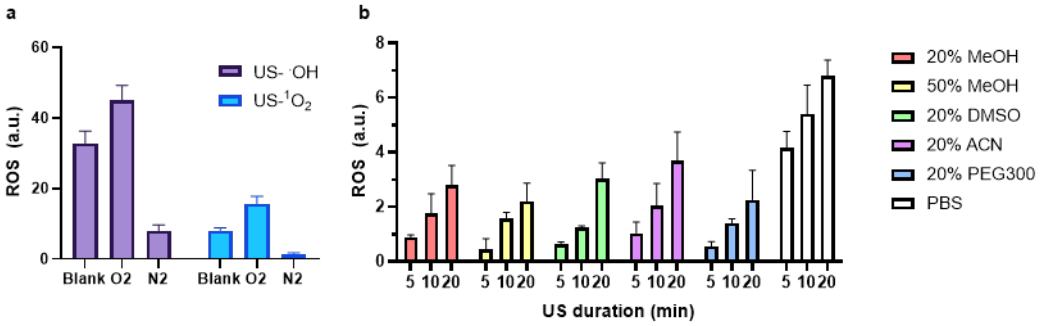

Supplementary Fig. 19 | Effects of gas atmosphere and solvent composition on ultrasound-generated ROS.

a, Influence of gas atmosphere on EPR-detected ROS generation. **b,** Influence of solvent composition on EPR-detected ROS generation. These data further demonstrate that cavitation chemistry is strongly modulated by the reaction environment.

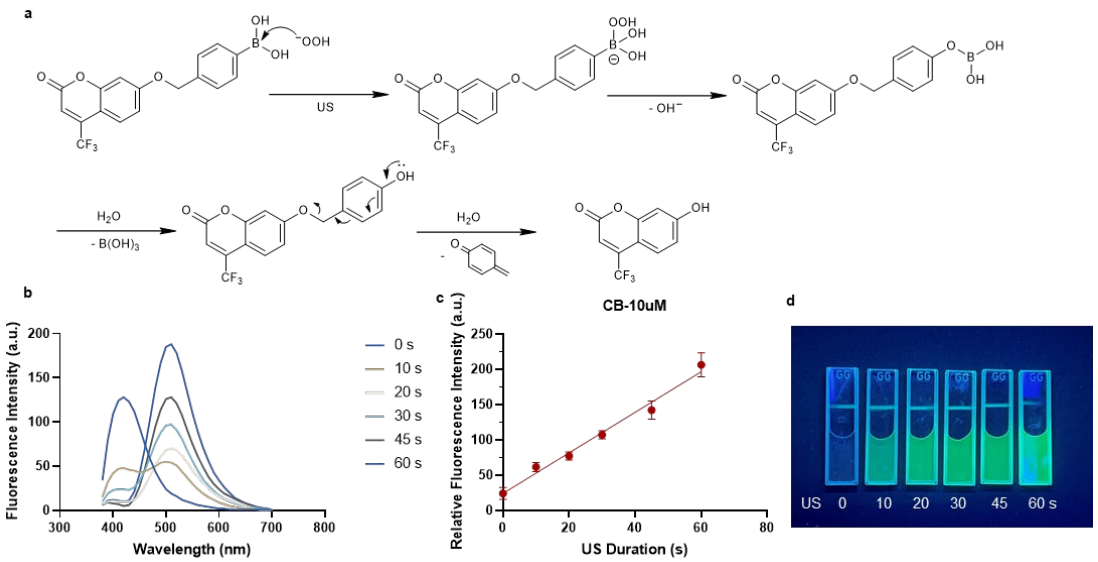

Supplementary Fig. 20 | Ultrasound-triggered activation of the boronic acid-caged coumarin probe CB.

a, Proposed fluorogenic activation scheme of CB under ultrasound. **b–d,** Time-dependent fluorescence increase of CB after ultrasound irradiation, demonstrating efficient probe activation.

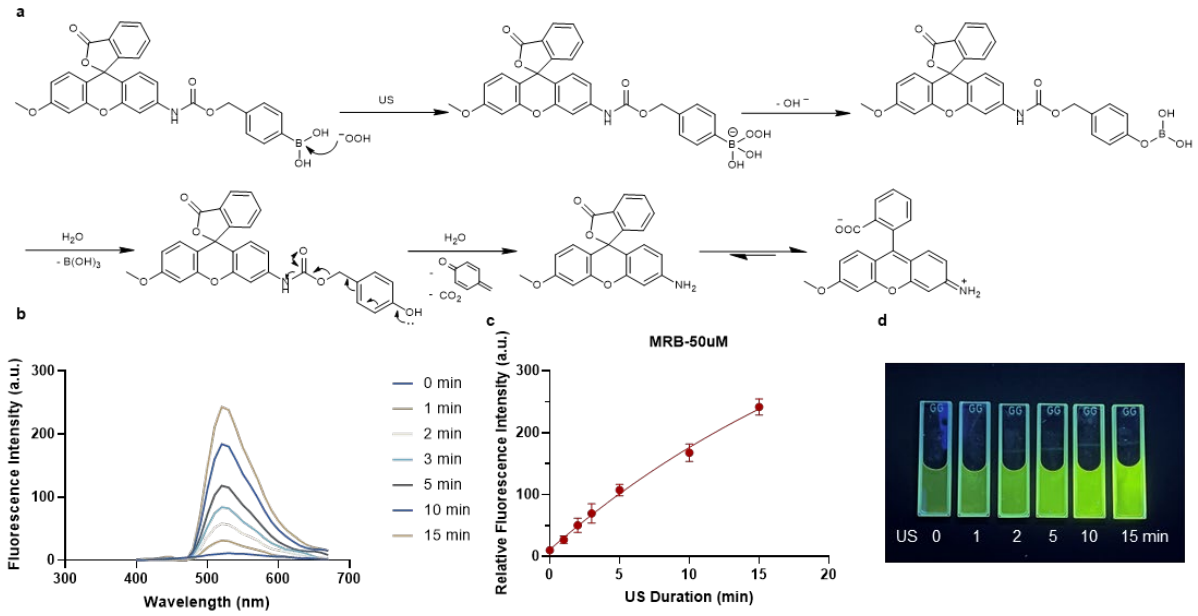

Supplementary Fig. 21 | Ultrasound-triggered activation of the boronic acid-caged fluorescein probe MRB.

a, Proposed fluorogenic activation scheme of MRB under ultrasound. **b–d,** Time-dependent fluorescence increase of MRB after ultrasound irradiation, demonstrating efficient fluorogenic decaging.

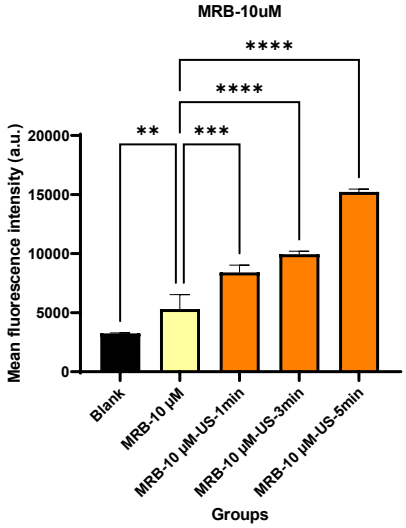

Supplementary Fig. 22 | Flow-cytometric analysis of ultrasound-triggered MRB activation in 4T1 cells.

Cells incubated with MRB show ultrasound-dependent fluorescence increase, supporting intracellular activation of the boronic acid-caged probe.

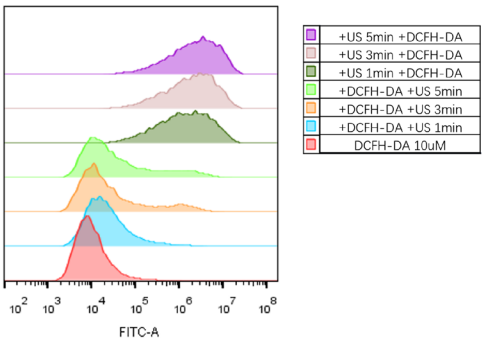

Supplementary Fig. 23 | Flow-cytometric analysis of ultrasound-triggered DCF activation in 4T1 cells.

Cellular fluorescence increases after ultrasound treatment, providing an additional ROS-responsive fluorescent readout in living cells.

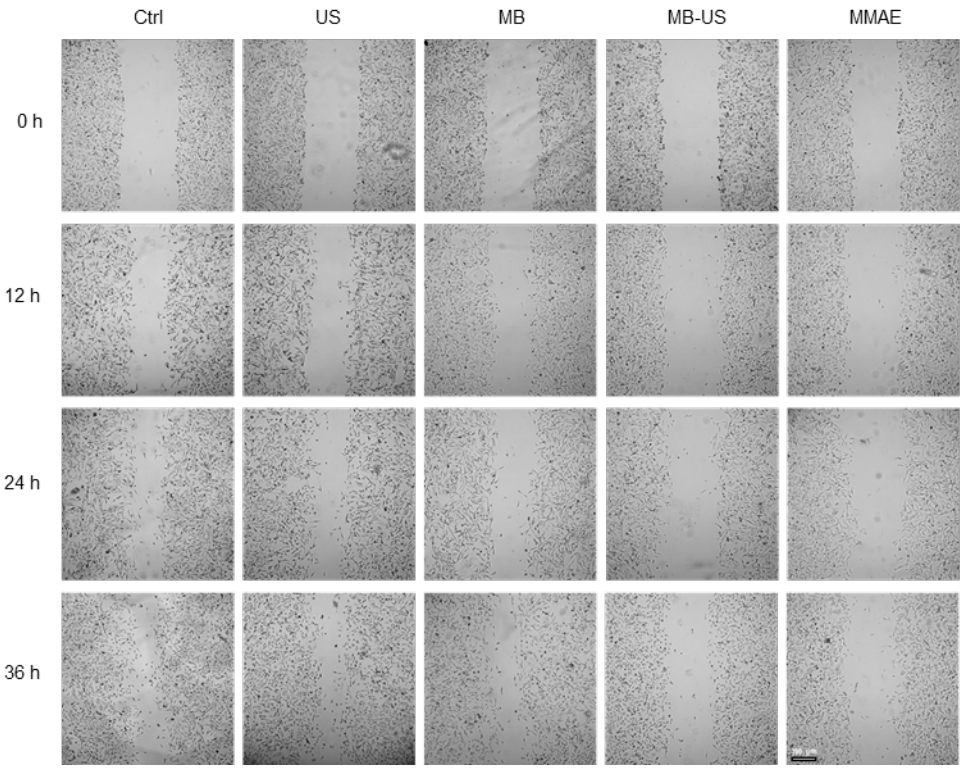

Supplementary Fig. 24 | Scratch assay evaluating ultrasound-triggered activation of MB in 4T1 cells.

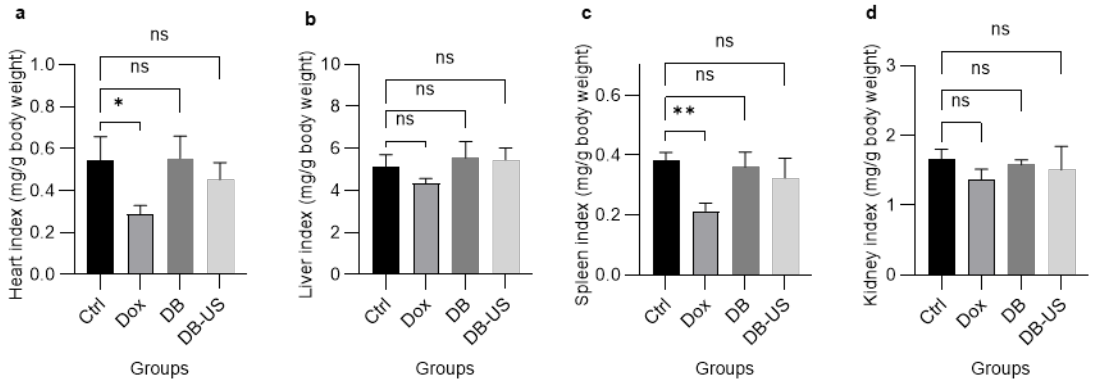

Supplementary Fig. 25 | Organ-index analysis after acute-toxicity evaluation of DB in 4T1 tumor-bearing mice.

Organ-weight indices were measured after DB treatment to assess acute systemic toxicity associated with ultrasound-triggered doxorubicin prodrug activation.

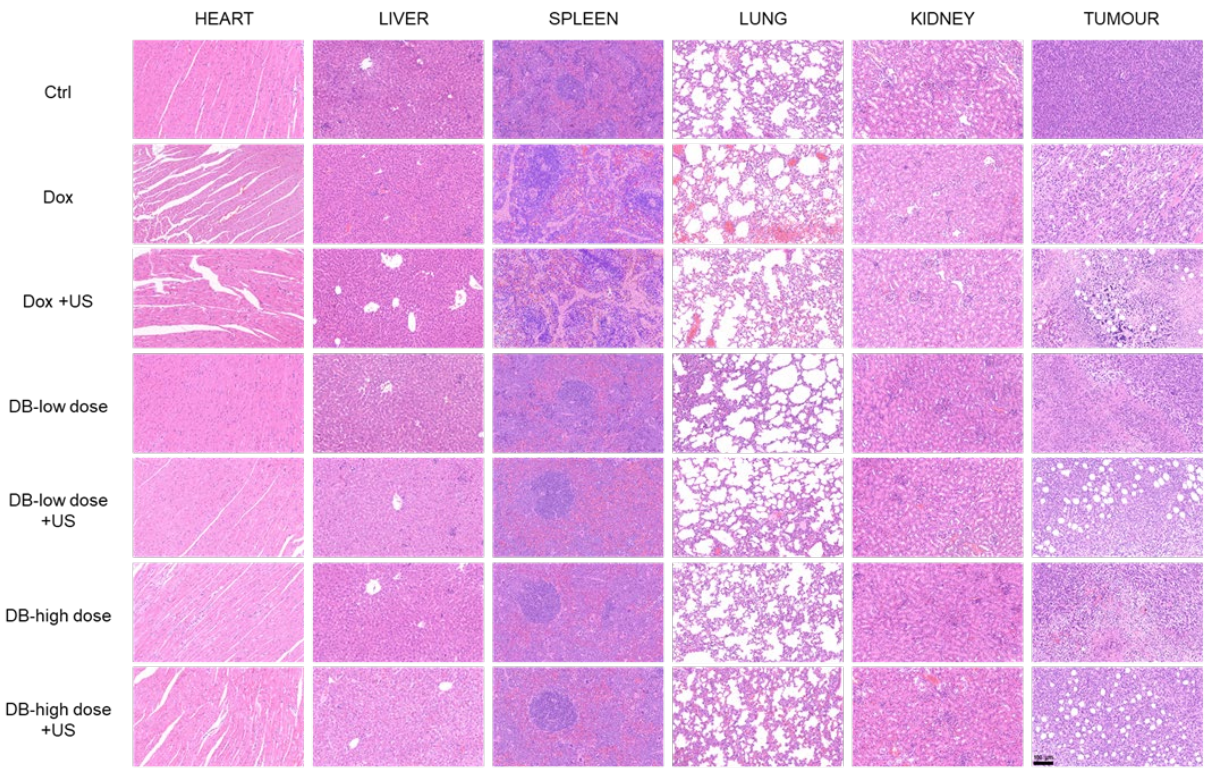

Supplementary Fig. 26 | Histological analysis of organs and tumors after DB treatment in 4T1 tumor-bearing mice.

Representative H&E staining of major organs and tumor tissues provides histopathological evaluation of treatment-associated efficacy and systemic toxicity.

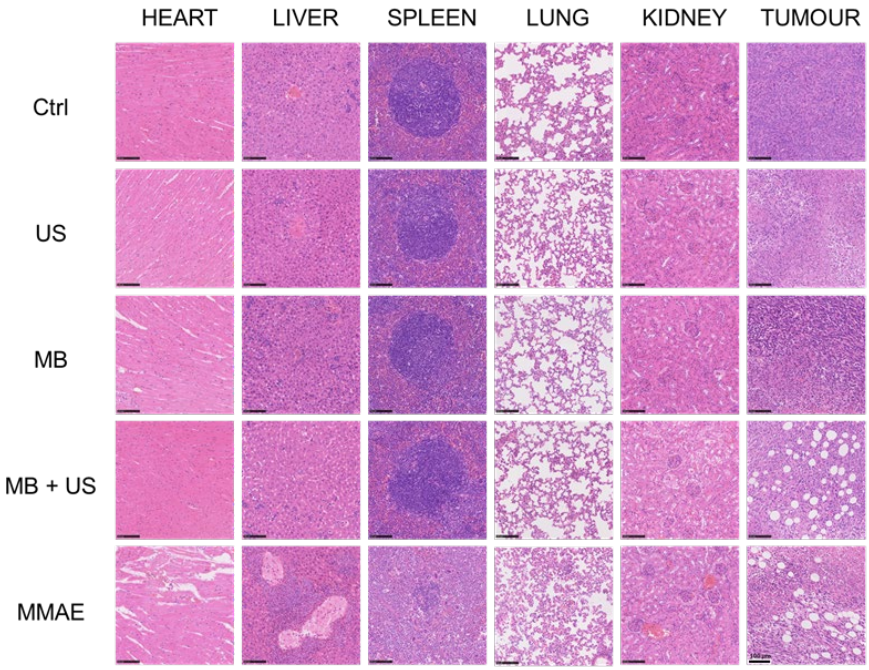

Supplementary Fig. 27 | Histological analysis of organs and tumors after MB treatment in 4T1 tumor-bearing mice.

Representative H&E staining of major organs and tumor tissues after MB-based therapy evaluates tissue-level therapeutic effect and safety.

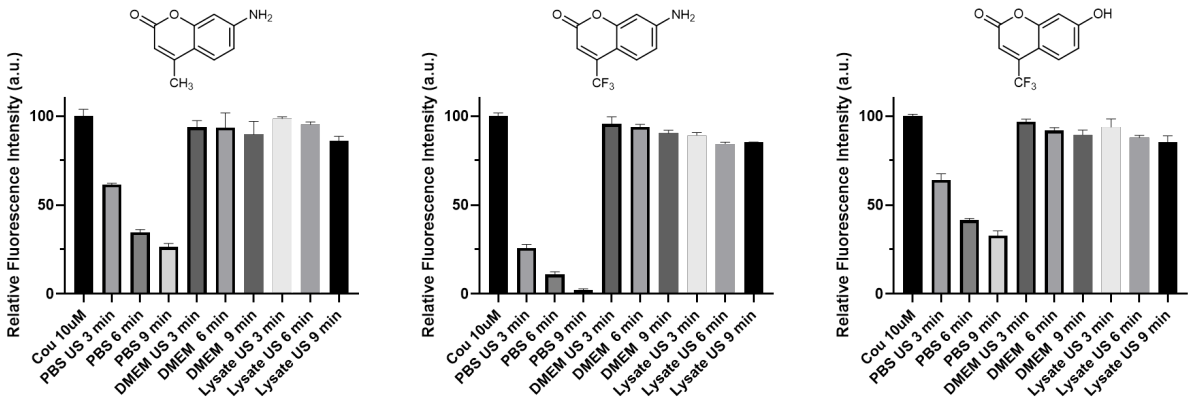

Supplementary Fig. 28 | Fluorescence decay of coumarin during ultrasound irradiation and modulation by reductive conditions.

Coumarin fluorescence decreases during ultrasound exposure because of hydroxyl-radical-mediated degradation in PBS, whereas reductive additives slow this decay, consistent with suppression of transient radical chemistry.

4. NMR and HRMS Spectra

Compound **1**: HRMS

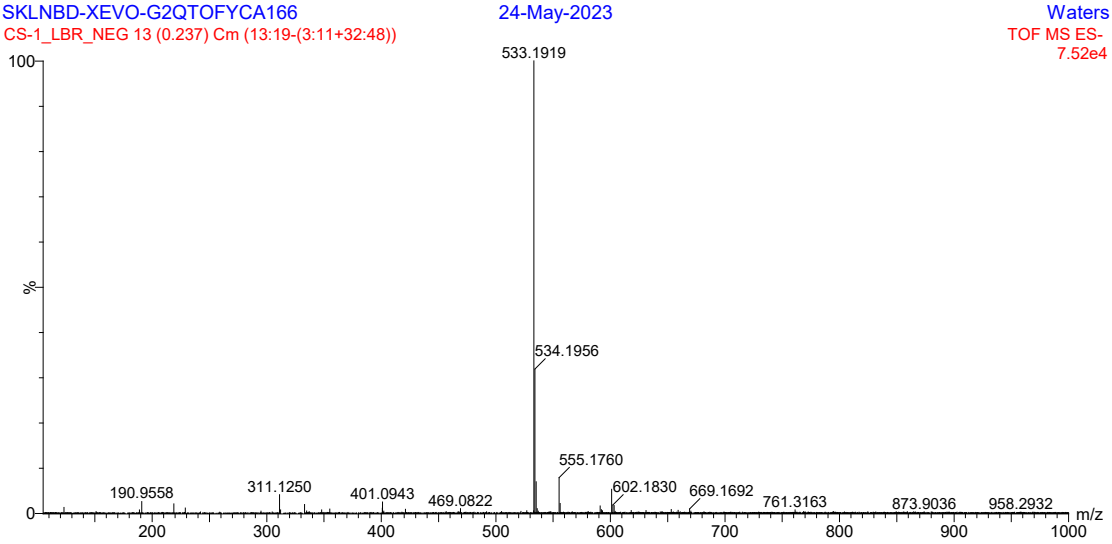

Compound **2**: ^{1}H NMR (400 MHz, $CDCl_3$)

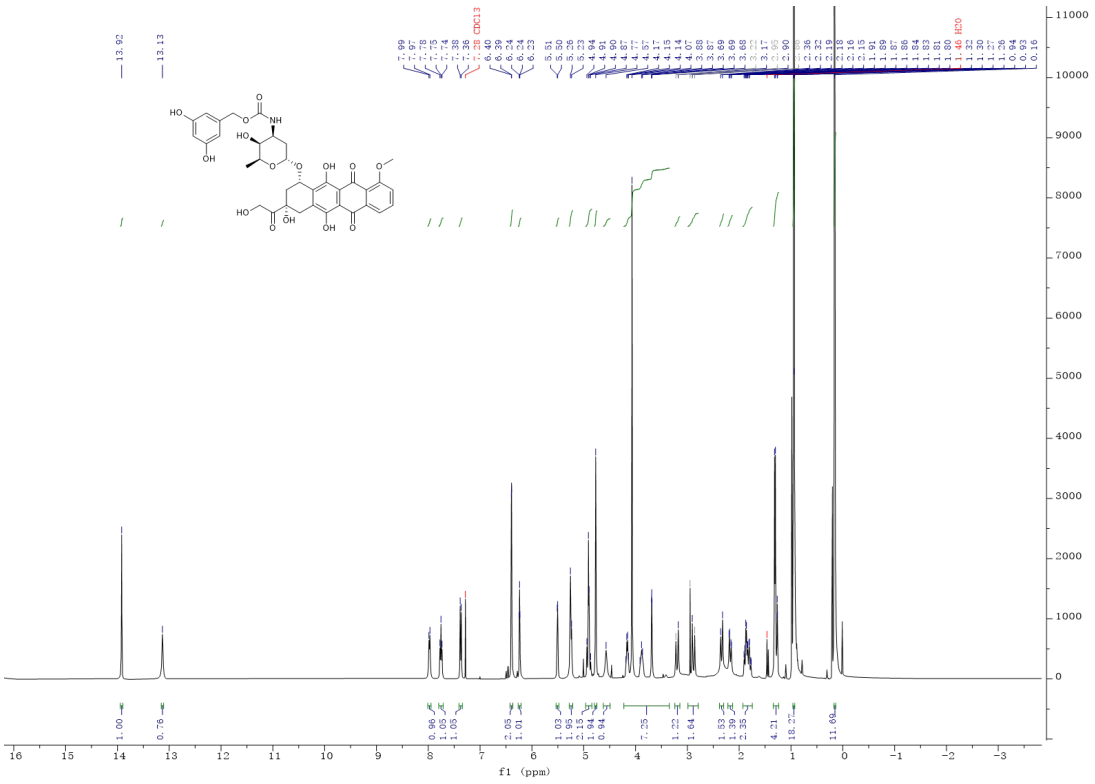

Compound **2**: ^{13}C NMR (101 MHz, $CDCl_3$)

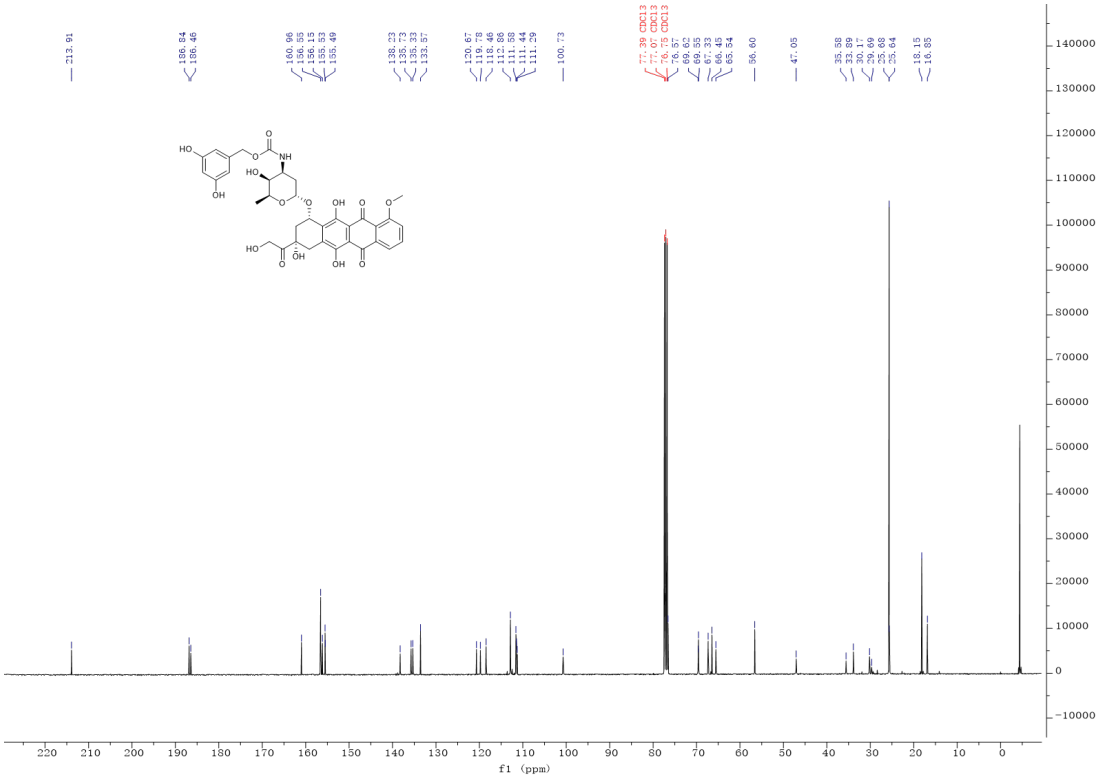

Compound **3**: HRMS

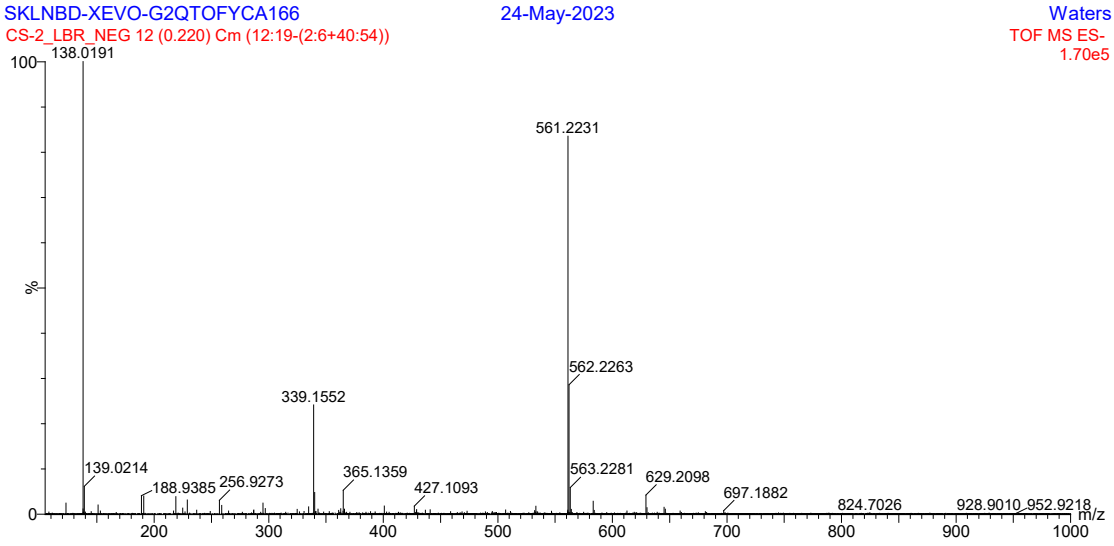

Compound **6**: ^{1}H NMR (400 MHz, $CDCl_3$)

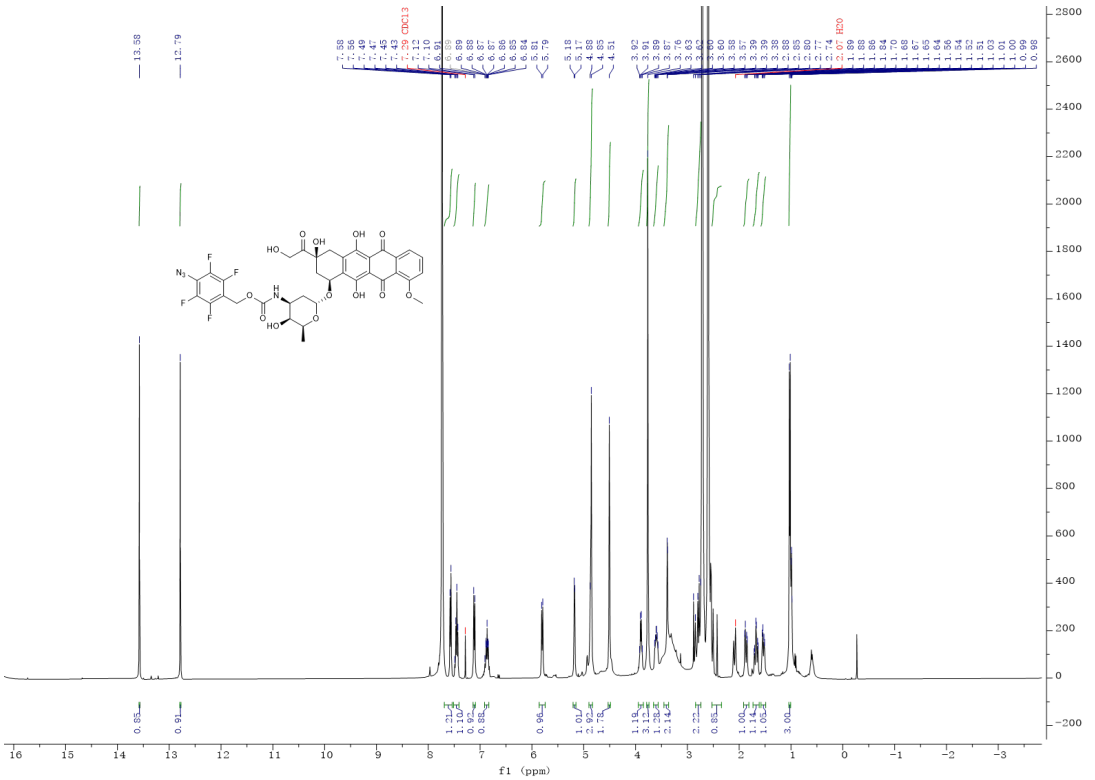

Compound **6**: ^{13}C NMR (101 MHz, $CDCl_3$)

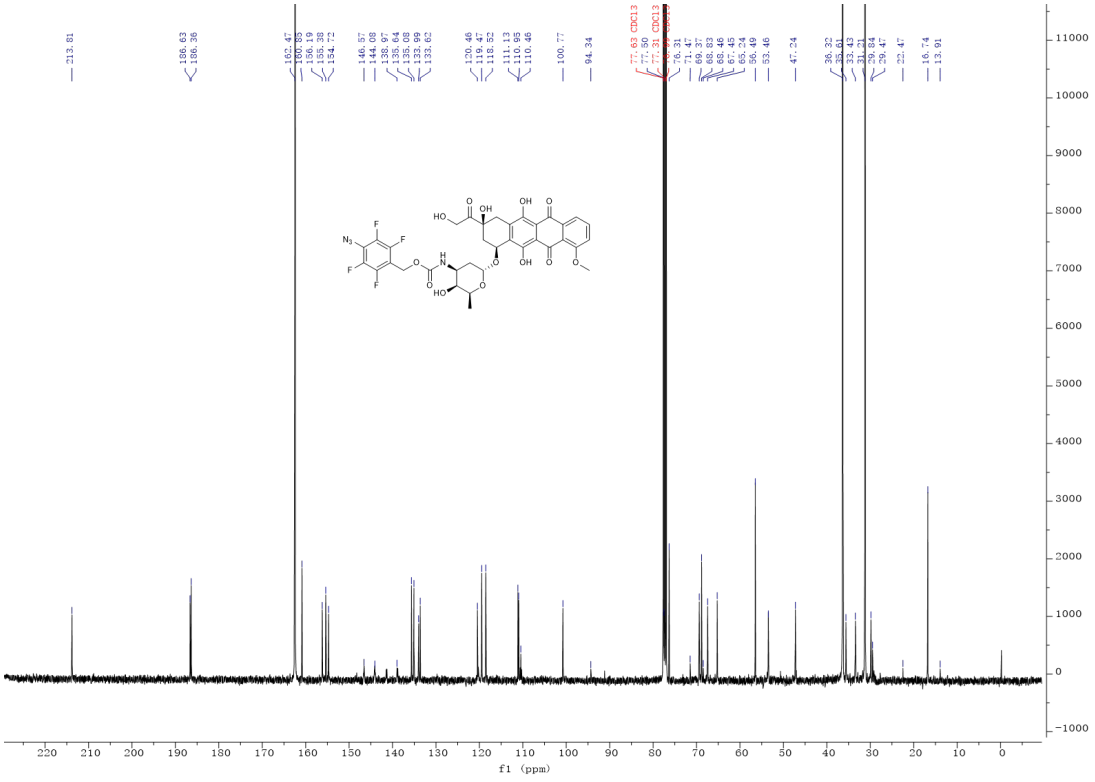

Compound **6**: HRMS

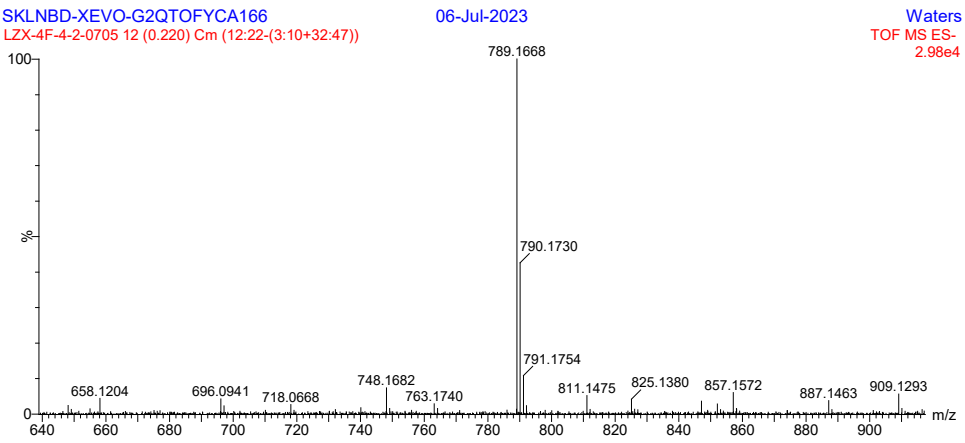

Compound **11**: ^{1}H NMR (400 MHz, DMSO-d_6)

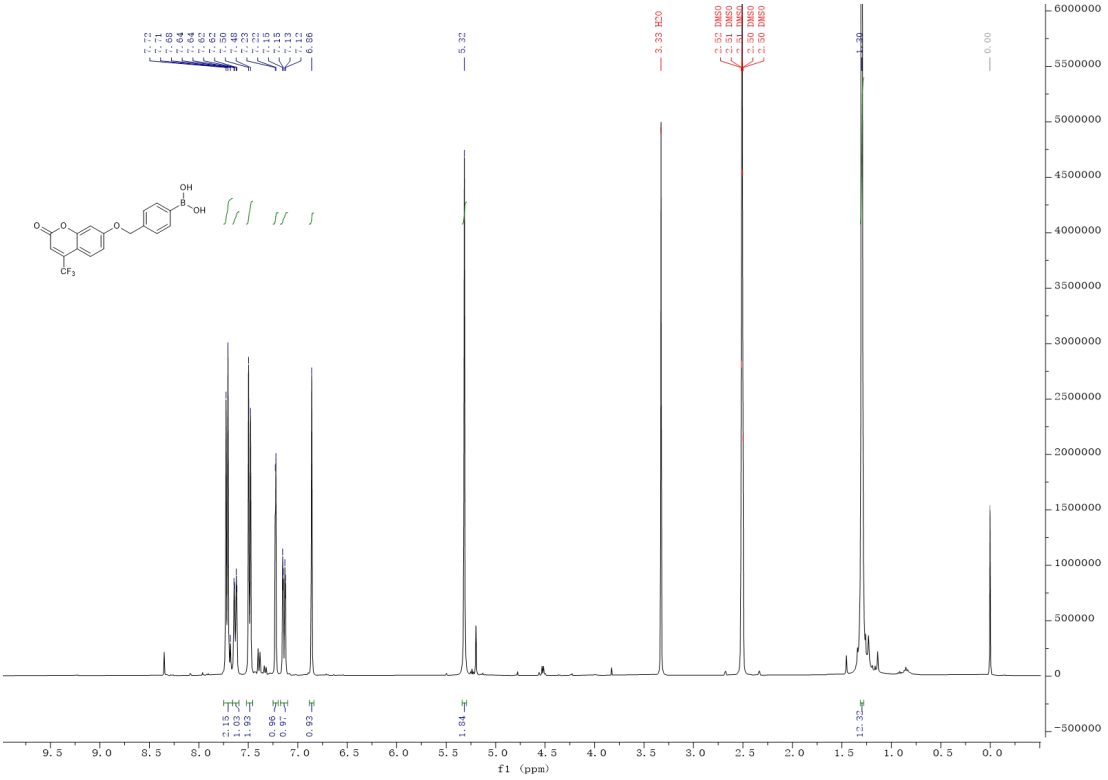

Compound **11**: ^{13}C NMR (101 MHz, DMSO-d_6)

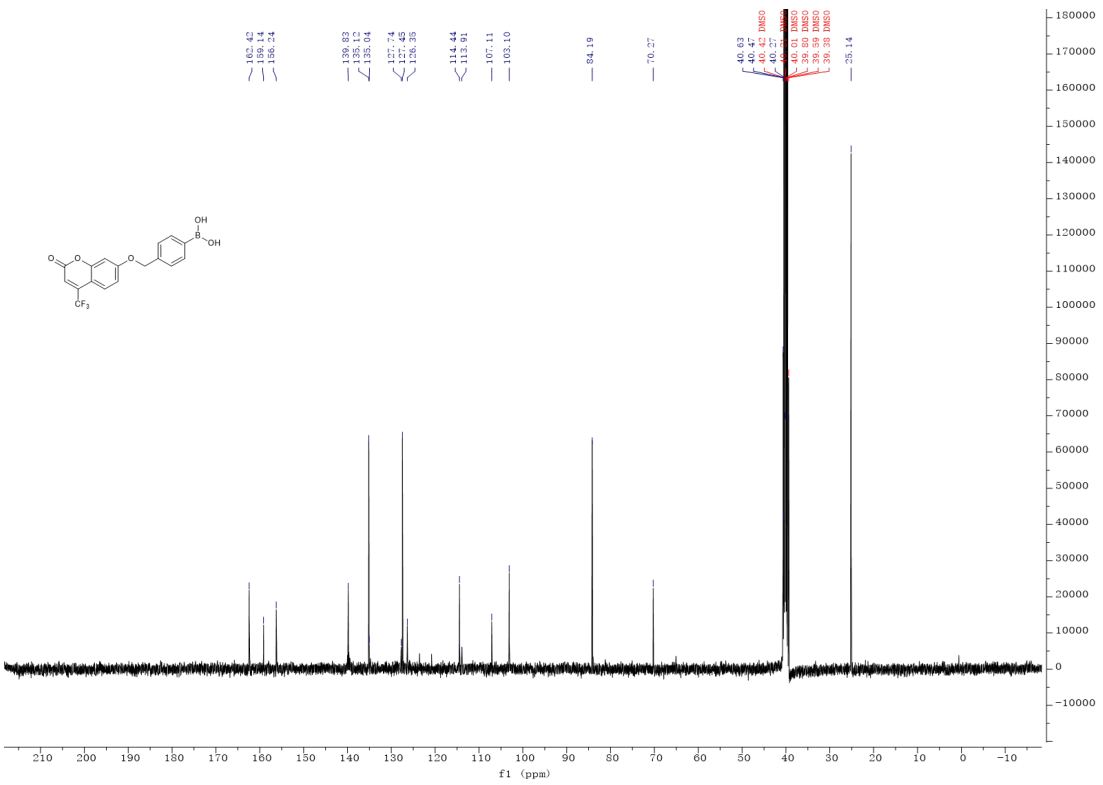

Compound **15**: ^{1}H NMR (400 MHz, DMSO-d_6)

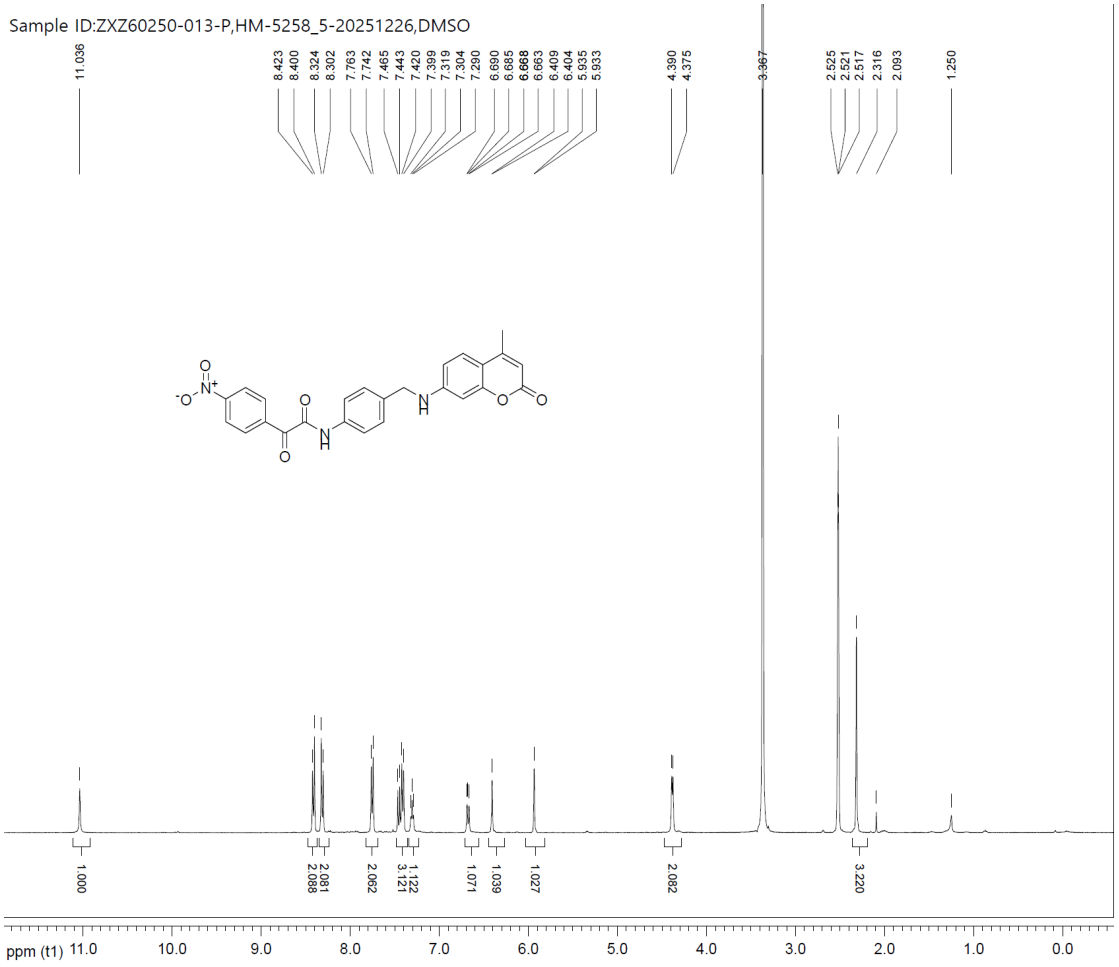

Compound **15**: ^{13}C NMR (101 MHz, DMSO-d_6)

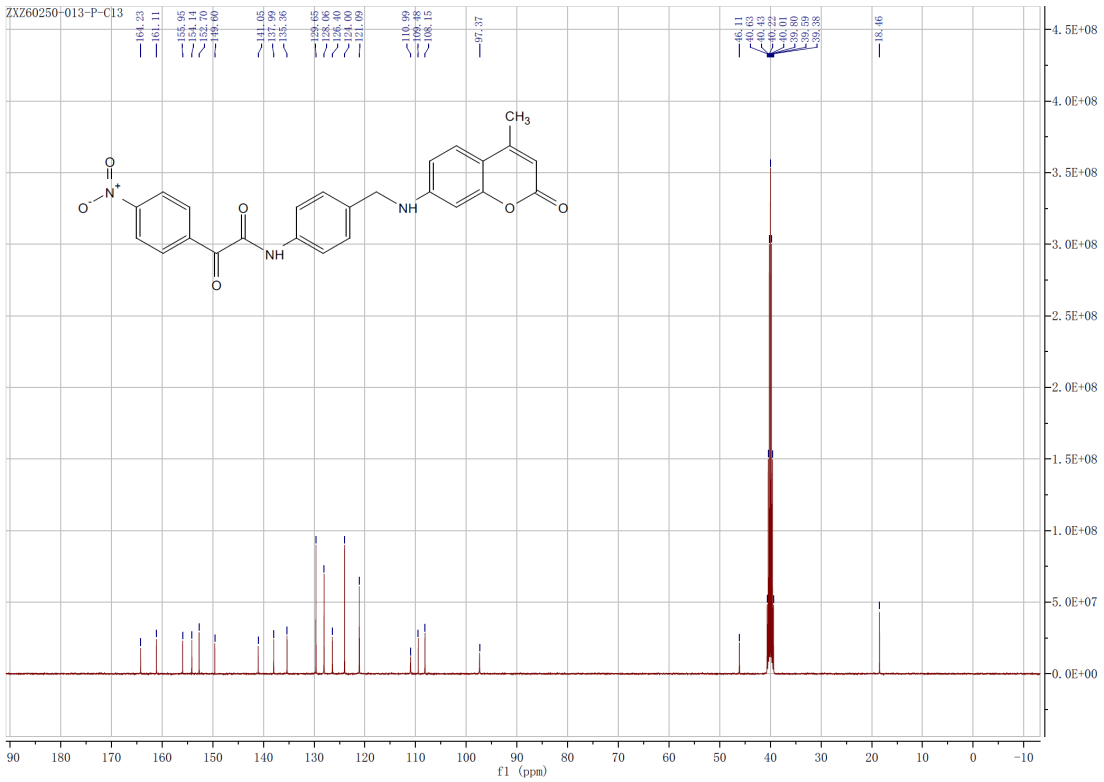

Compound **16**: ^{1}H NMR (400 MHz, DMSO-d_6)

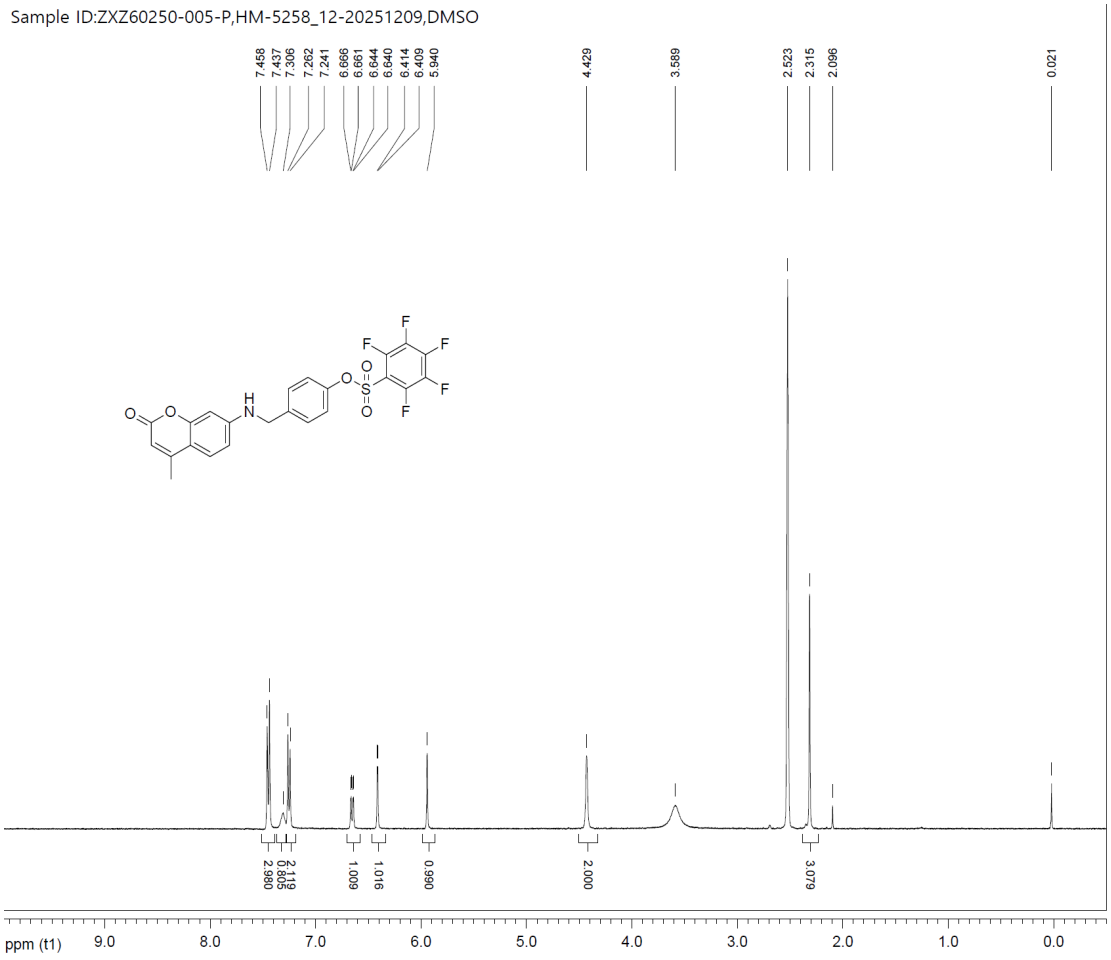

Compound **18**: ^{1}H NMR (400 MHz, $CDCl_3$)

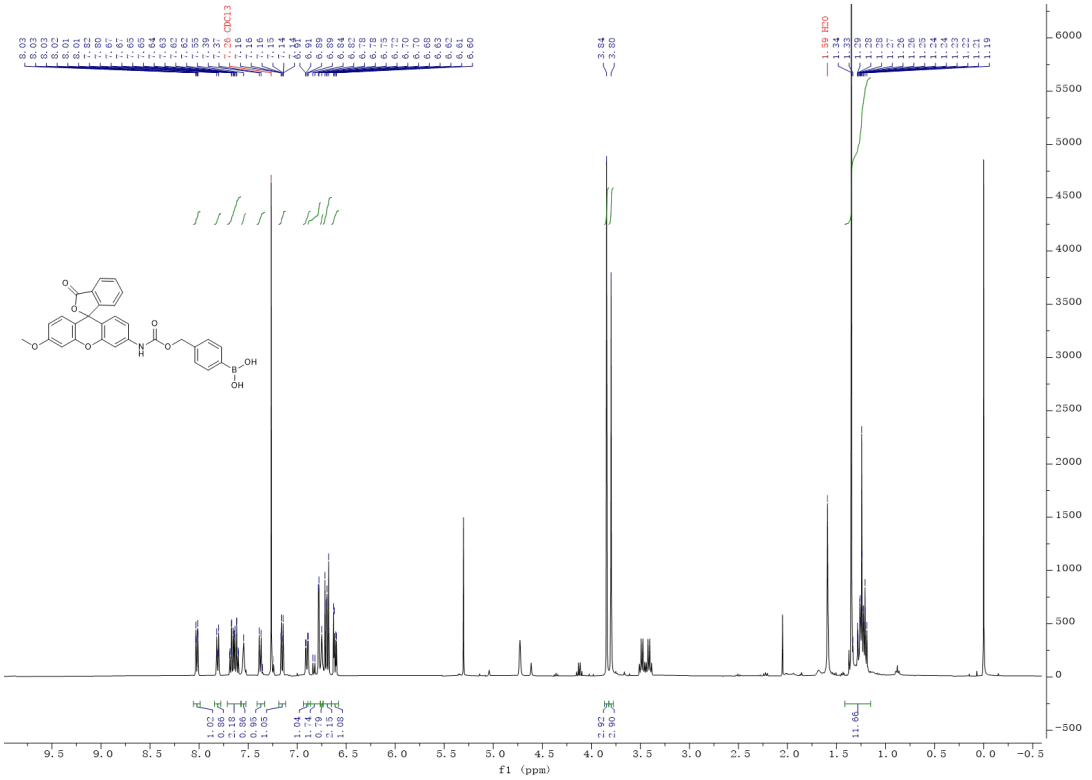

Compound **19**: ^{1}H NMR (400 MHz, DMSO-d_6)

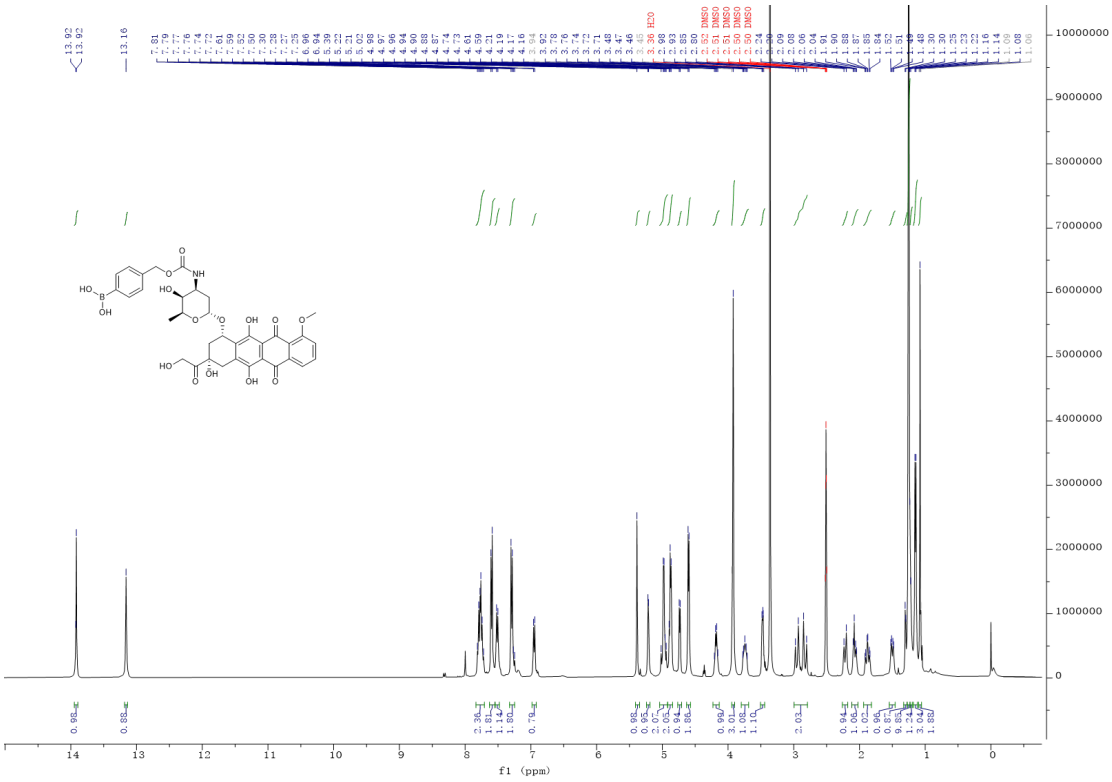

Compound **19**: ^{13}C NMR (101 MHz, DMSO-d_6)

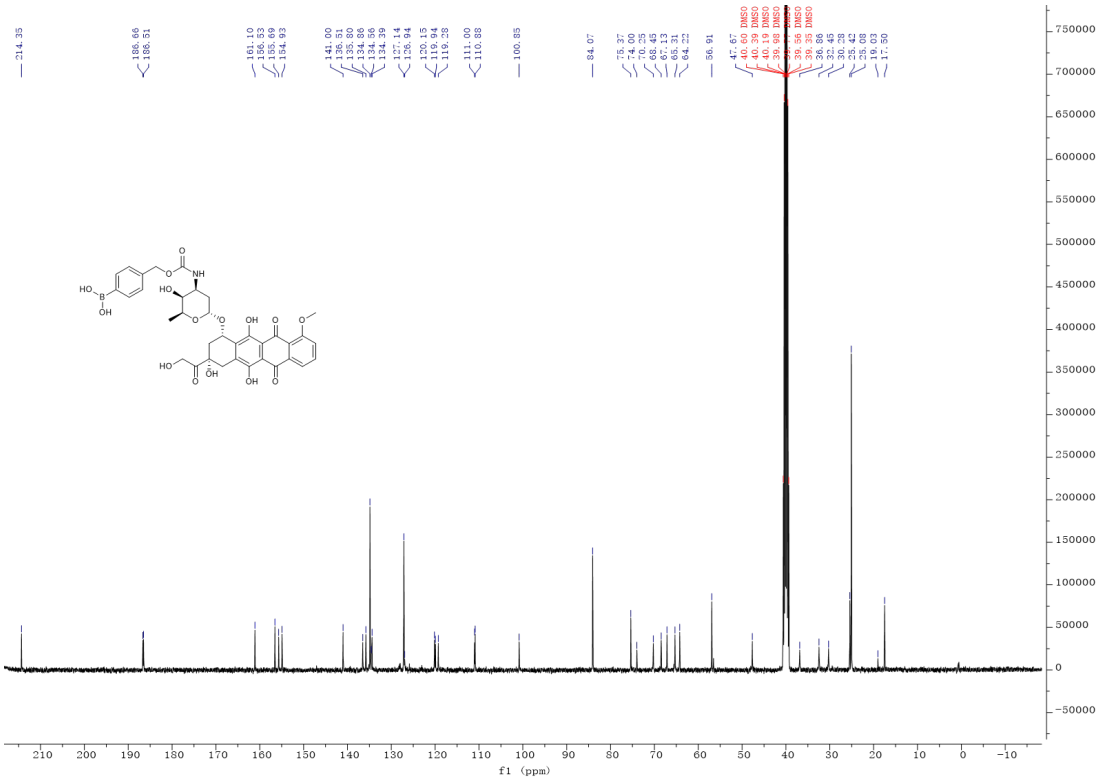

Compound **20**: ^{1}H NMR (400 MHz, CD_3OD_SPE)

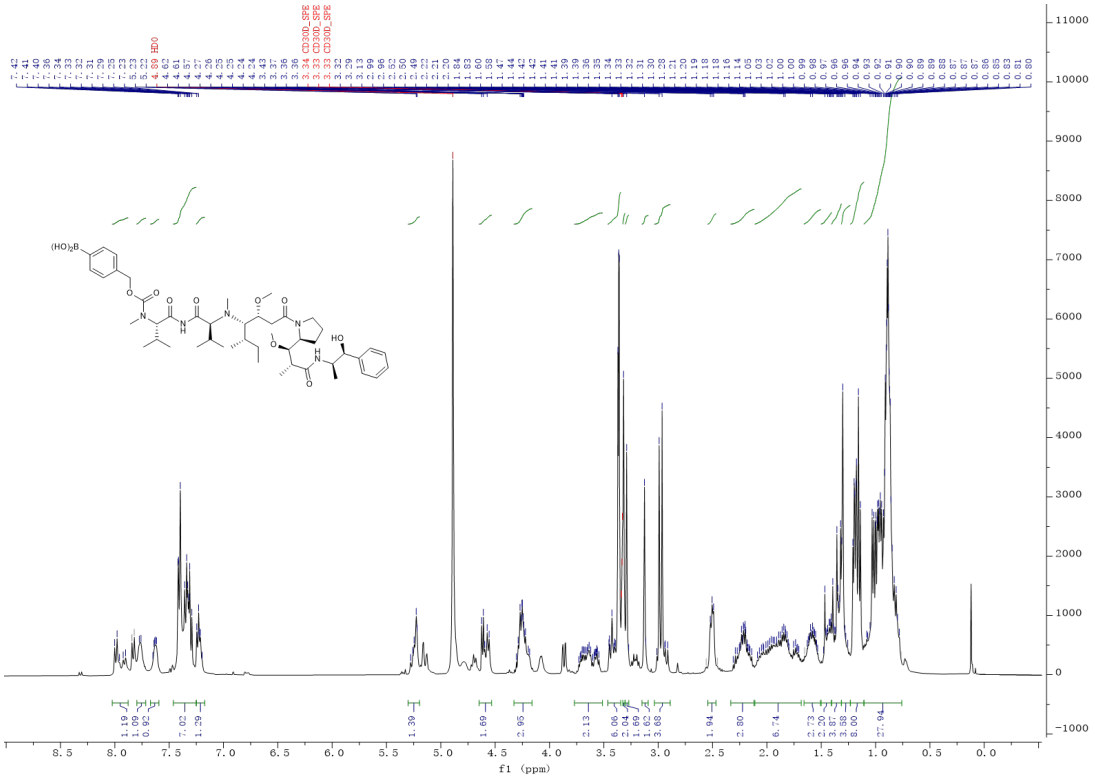

Compound **20**: ^{13}C NMR (101 MHz, CD_3OD_SPE)

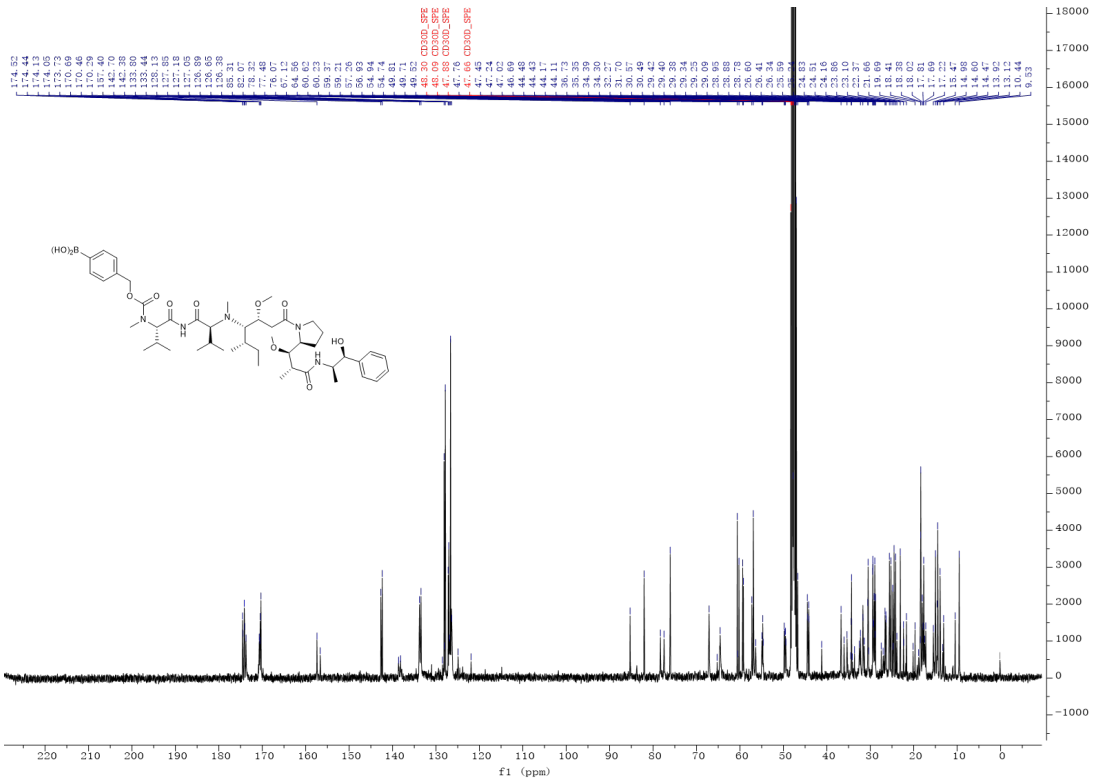

Compound **21**: ^{1}H NMR (400 MHz, DMSO-d_6)

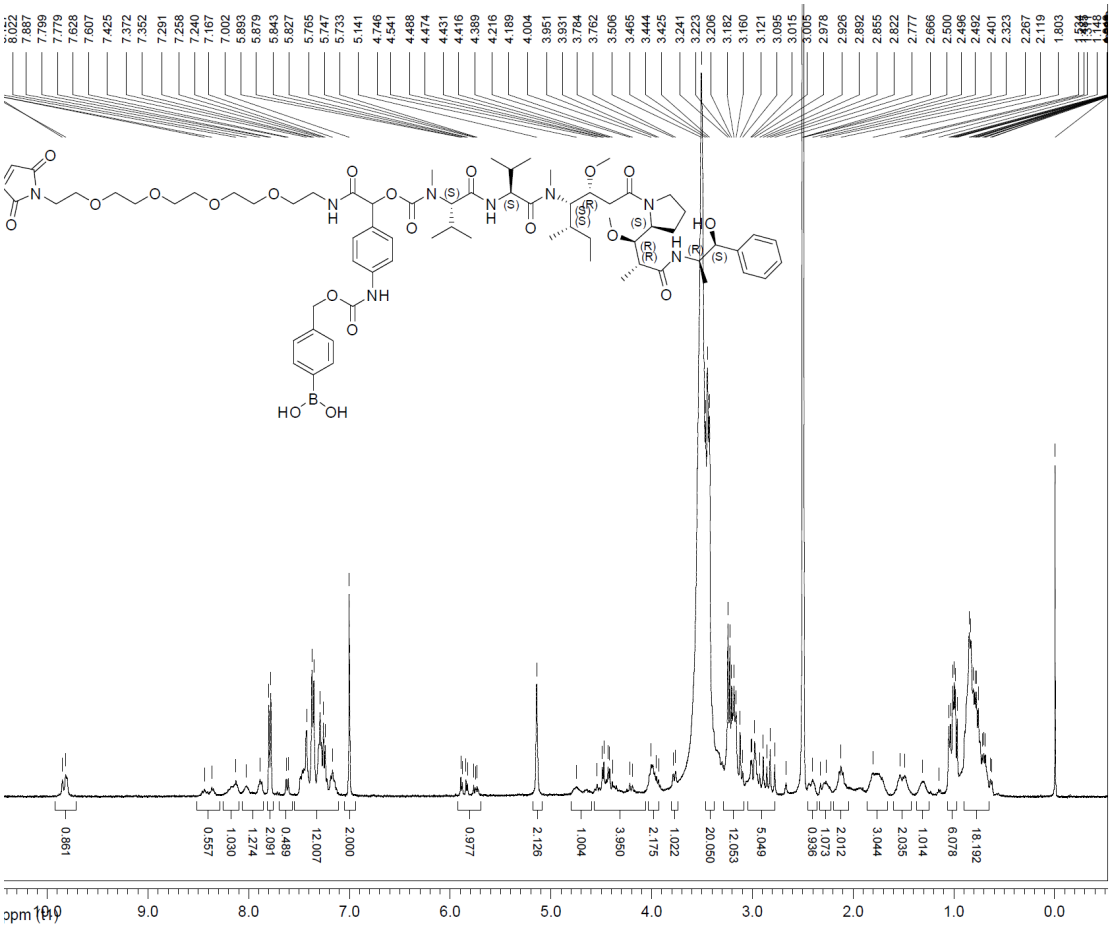

Compound **21**: ^{13}C NMR (101 MHz, CD_3OD_SPE)

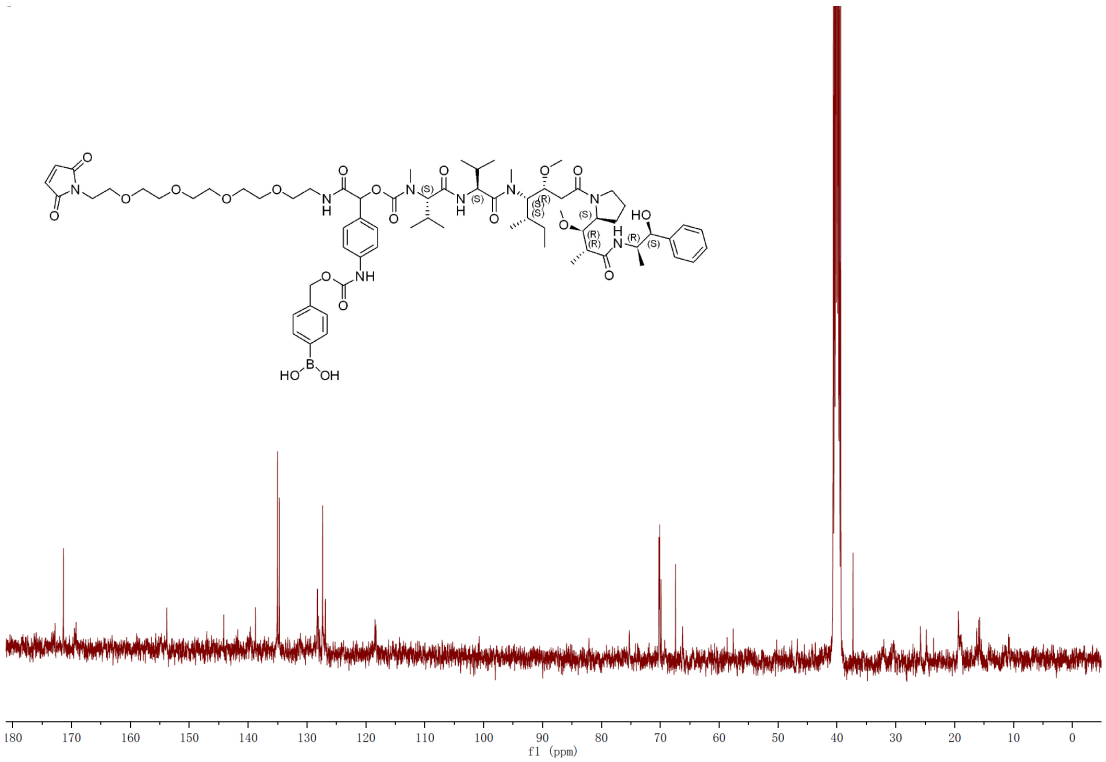

5. References

[1] Geng, J. *et al.* Switching on prodrugs using radiotherapy. *Nat Chem* **13**, 805-810, doi:10.1038/s41557-021-00711-4 (2021).